UC Santa Cruz

UC Santa Cruz Electronic Theses and Dissertations

Title

Functional Characterization of Retinal Ganglion Cells in the Wild-Type and Mutant Mouse

Permalink

https://escholarship.org/uc/item/4w30t997

Author

Ng, Arash

Publication Date

2014

Peer reviewed|Thesis/dissertation

eScholarship.org Powered by the California Digital Library
University of California

UNIVERSITY OF CALIFORNIA
SANTA CRUZ

FUNCTIONAL CHARACTERIZATION OF RETINAL GANGLION CELLS IN THE WILD-TYPE AND MUTANT MOUSE

A dissertation submitted in partial satisfaction
of the requirements for the degree of

DOCTOR OF PHILOSOPHY

in

MOLECULAR, CELL AND DEVELOPMENTAL BIOLOGY

by

Arash Ng

June 2014

The Dissertation of Arash Ng is
approved:

_____
Professor David Feldheim, chair

_____
Professor Alexander Sher

_____
Professor Bin Chen

_____
Tyrus Miller
Vice Provost and Dean of Graduate Studies

Copyright © by

Arash Ng

2014

Table of Contents

List of Figures

Figures

Abstract

Arash Ng

FUNCTIONAL CHARACTERIZATION OF RETINAL GANGLION CELLS IN THE WILD-TYPE AND MUTANT MOUSE

The retina extracts relevant features from the visual scene and transmits these features to the brain through separate pathways that will eventually result in the perception of sight. The retinal ganglion cells (RGCs) are the only retinal cell type to send an axonal projection to the brain. This indicates that the signals generated by the RGCs are the end result of retinal processing, and the features detected by the RGCs are all that will be transmitted to the brain about the visual environment. Each RGC type represents a unique pathway that detects specific visual features. RGCs of the same type tile the retina so that the entire visual field is sampled. Different types of RGCs overlap so that each pixel in the visual field gets sampled by each pathway. To understand the different retinal pathways and what gets sent to the brain, it is necessary to know what types of RGCs are in the retina. Current classifications have used morphologies and physiology to describe the different RGC types. It is estimated that 20 different types of RGCs are present in the mammalian retina. However, very little is known about how these morphological features affect functional properties due to the inability to perturb the morphology and observe changes in physiology in many mammals. In order to overcome this limitation, I utilized a large-scale multielectrode array (MEA) approach to record and characterize

responses from hundreds of RGCs in the mouse retina. The mouse model is advantageous due to the ease of genetic manipulation, allowing me to disrupt morphology and relate the changes to function. I first characterized and classified RGCs in the wild-type retina to develop a reference for mutant comparisons. I was able to classify up to 8 types of RGCs along with functional properties of the classes, such as tiling arrangements of the RGC receptive fields (RFs). Using a mutant mouse that has defects in dendritic and cell body spacing, I show that the dendritic structure is important for RF tiling and direction selective responses thus showing how morphology affects function. Finally, I used a transgenic mouse, in which RGCs expressing a particular gene was ablated, to show that these eliminated RGCs were a distinct functional subset that responded to light offset. The work that I performed will contribute to a complete classification of RGCs by linking the morphological types to the functional types, as well as the genetic programs that establish their properties. This will be necessary to determine what features are detected by the retina and how they ultimately lead to behavior.

Acknowledgements

I would like to acknowledge the people who made this work possible. First I would like to thank my advisers Dr. David Feldheim and Dr. Alexander Sher for their constant support, academically, financially, and personally. I also would like to thank the members of both labs for the discussion and assistance they provided me throughout my graduate career. Dr. Alan Litke and Dr. Shinya Ito provided input and technical support for use of the MEA and the custom software designed for it. Dr. Bin Chen served on my thesis committee. I would like to thank Erin Zampaglione for performing analysis on the direction selective stimuli. Additionally, I would like to thank Dr. Peter Fuerst and Dr. Robert Burgess for their collaboration and generously donating the DSCAM KO animals. Chapter 2 comes from a manuscript that I have written and has not yet been submitted for peer review. Support for my work was provided by NIH and the MCD Biology department at UCSC. Finally, I would like to thank my parents and brother who have always been my greatest supporters in life. Without all these people, and many others too numerous to include, I would not be where I am today.

Introduction

The visual system is responsible for transforming light energy into electrical potentials and interpreting these signals to generate behaviors. It performs these tasks through a multitude of cell types organized into different circuits. Each cell type has a specialized function for detecting and transmitting one or more features of the visual scene. These features are encoded by electrical signals that the brain uses to generate our visual experience.

Vision begins in the eye

Vision begins in the eye where incoming light from the environment is focused onto the retina (Figure 1). Light enters the eye through the cornea and pupil of the iris. The light then is focused onto the retina by the lens. Light also passes through two fluid filled chambers, the aqueous humor, between the cornea and lens, and the vitreous humor, between the lens and the retina. The retinal pigment epithelium lines the back of the retina and is important for a number of functions including photoreceptor maintenance and reducing light scatter.

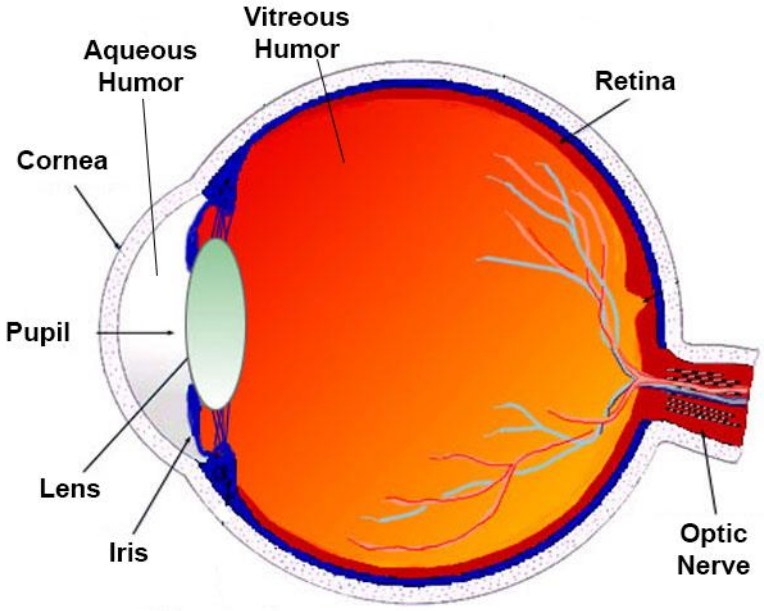

Figure 1. A diagram of a cross section of an eyeball (adapted from Wikipedia).

The retina is part of the central nervous system.

The retina is the light sensitive neural tissue that lines the back of the eye. The retina consists of 5 main cell types: photoreceptors, bipolar cells, horizontal cells, amacrine cells and retinal ganglion cells (RGCs) (Figure 2). Müller glial cells are the main glia in the retina. These cell types are organized into five discrete layers. The outer nuclear layer (ONL) consists of cell bodies of photoreceptors, the main photon detectors in the retina. The inner nuclear layer (INL) consists of cell bodies from bipolar, horizontal and amacrine cells, collectively termed the interneurons of the retina. The ganglion cell layer (GCL) consists of cell bodies of the RGCs as well as displaced amacrine cells. The ONL is located near the back of the eye, whereas the GCL is located near the middle, or inner portion, of the eye. Photoreceptors, bipolar

and horizontal cells form synapses in the outer plexiform layer (OPL, which is located between the ONL and INL. In the inner plexiform layer (IPL), located between the INL and GCL bipolar and amacrine cells synapse onto RGCs.

For several reasons, the retina is particularly well-suited to the study of how neural function is related to circuit properties. The retina is part of the central nervous system (CNS) and shares anatomical features with other CNS structures, such as laminar structure. It is likely that what is found in the retina can apply to other CNS structures due to the anatomical similarities. Unlike other CNS structures, the retina is readily accessible to dissection and experimental manipulations. Importantly, the retina has well defined input stimuli (light) and output responses (RGC action potential activity), which facilitate studies of neural function.

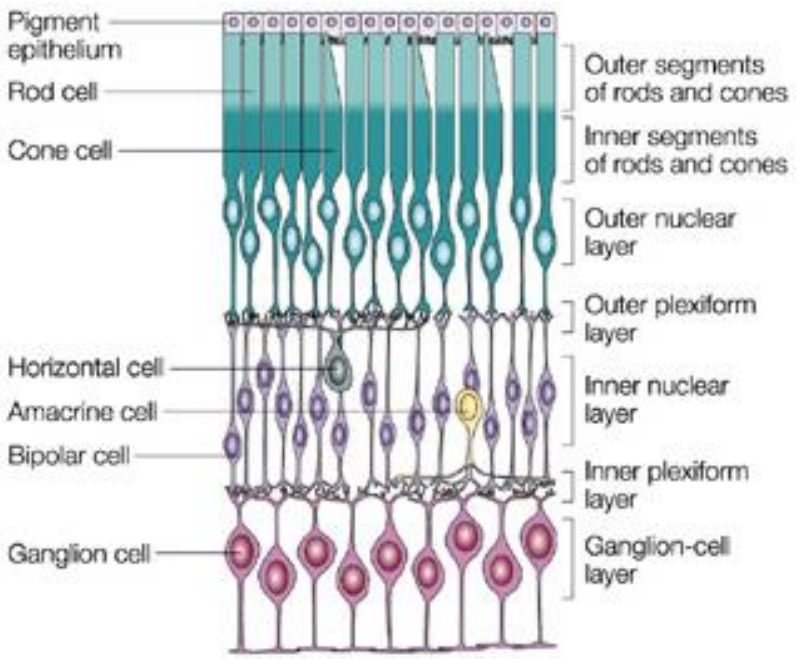

Figure 2. A schematic view of the retina with the cell types labeled (Carroll et al., 2004).

Phototransduction and synaptic transmission in the retina

The process of phototransduction converts light information into electrical signals and is reviewed elsewhere (Purves, 2008). Photoreceptors are positioned in the outer retina near the back of the eye, while RGCs reside in the inner retina. Because of this inverted arrangement, light must first pass through all the layers of the retina before reaching the photoreceptors. Photons are absorbed by opsins, the light absorbing photo pigments, present in the photoreceptors. The opsins are converted from an 11-*cis* conformation to an all *trans* conformation. This leads to a signal transduction cascade that will close cation channels embedded in the photoreceptor's membrane hyperpolarizing the cell and halting glutamate release.

Ultimately, photoreceptor activation leads to RGC signaling. When the photoreceptor terminal releases less glutamate the ON type bipolar cells postsynaptic to it is depolarized. In the dark, the photoreceptor's membrane potential is more depolarized and releases more glutamate in the dark. This results in OFF type bipolar cells becoming more depolarized. The difference in the responses of the bipolar cell types relies on the expression of different glutamate receptors. The ON and OFF type bipolar cells synapse onto ON and OFF type RGCs, respectively. An active (i.e. depolarized) bipolar cell will activate its respective RGC. The RGCs convert signals from the interneurons into trains of action potentials and transmit these spike trains to the visual centers in the brain. The photoreceptor to bipolar to RGC pathway is the most common and direct transmission of light information (Figure 3). The horizontal

cells provide lateral inhibition between the photoreceptor and bipolar cell synapse, while the amacrine cells provide lateral inhibition between the bipolar and RGC synapse.

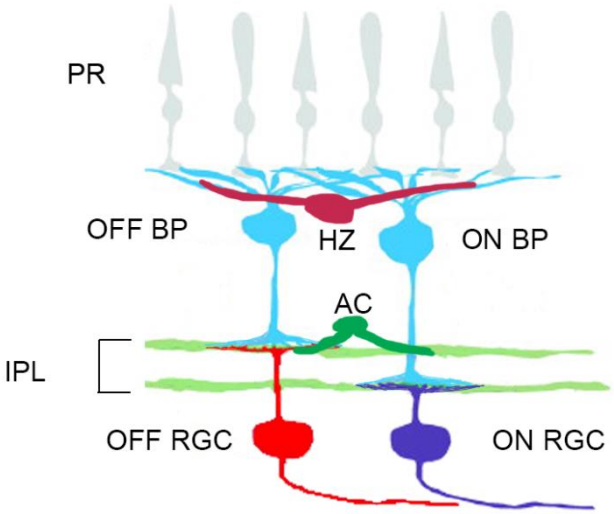

Figure 3. A schematic of the synaptic connections in the retina (adapted from Wei and Feller, 2011). Direct transmission is accomplished by the photoreceptor (PR) to bipolar cell (BP) to RGC pathway. The horizontal cells (HC) provide lateral inhibition between the PR and BP synapses and the amacrine cell (AC) provide lateral inhibition between the BP and RGC synapses.

Parallel pathways

The retina is not a pixel detector like a camera, but instead extracts specific information from the visual field and transmits these signals through separate pathways. This is a common organizational strategy in sensory systems called parallel processing (Wassle, 2004; Nassi and Callaway, 2009). Visual features, such as contrast, color, and direction of motion, are transmitted via dedicated circuits in the

retina. Different pathways overlap in space so that the entire visual field can be sampled by every circuit. The basic unit of a circuit begins with a photoreceptor and ends at a specific type of RGC. By characterizing the functional properties of all of the RGC types, we can determine the visual features that are detected by the retina, and ultimately, how they contribute to visual perception and behavior.

Retinal ganglion cells and mosaics

The RGCs are the output neurons of the retina. RGCs generate action potentials and are the only retinal neuron to project axons to the brain. Therefore, the patterns of their action potentials represent the sum of retinal activation and processing. RGCs are not a homogenous population, but consist of ~22 distinct types based on morphological, anatomical, physiological features (Dacey, 1999; Sun et al., 2002; Kong et al., 2005; Coombs et al., 2006; Berson, 2008; Volgyi et al., 2009; Farrow and Masland, 2011; Masland, 2012). Currently, a complete and comprehensive classification of the different types of RGCs has not yet been achieved. In order to generate such a classification, each type of RGC must be described in terms of morphology, physiology and genetics.

Within the 2D plane of the GCL, RGCs of the same type are positioned to sample the entire visual field. Anatomically, RGCs of the same type arrange their cell bodies in regularly spaced mosaics with their dendrites tiling the space between them (Wassle et al., 1981; Rodieck, 1991; Rodieck and Marshak, 1992; Dacey, 1993b)

(Figure 4). Functionally, same type RGC receptive fields (RFs) also form mosaics across the visual space (Devries and Baylor, 1997; Shlens et al., 2006; Field et al., 2007; Petrusca et al., 2007; Gauthier et al., 2009; Anishchenko et al., 2010; Sher and DeVries, 2012) (Figure 5). This mosaic arrangement allows each circuit to sample the entire visual space with little overlap and no blind spots. As mentioned, different circuits must overlap in space if they are to sample the entire visual space. Mosaics from one type of RGC will overlap with the mosaic of another type. RGCs are not the only retinal cell type that form 2D mosaics. Subtypes of photoreceptors, bipolars and amacrine cells have been shown to form mosaics as well (Rodieck and Marshak, 1992; Fuerst et al., 2008; Wassle et al., 2009). Mosaic arrangement is a good indicator that cells are part of a unique subset. Hence, the mosaic principle can be used to verify classification of RGCs.

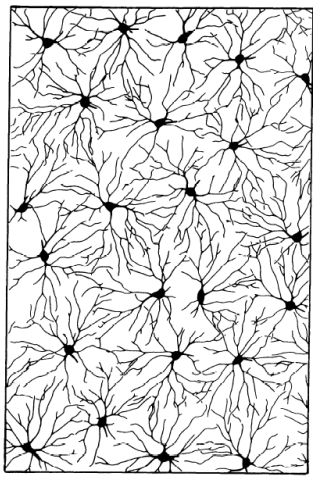

Figure 4. Mosaic arrangement of same type RGC cell bodies and tiling of dendrites (Wässle and Boycott, 1991).

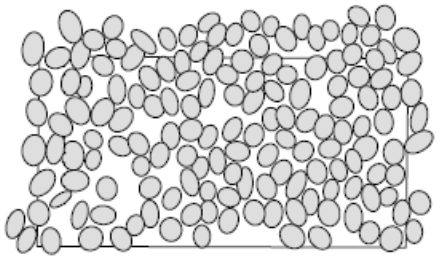

Figure 5. Mosaic arrangement of same type RGC receptive field identified by a large-scale multielectrode array. Circles represent the spatial RFs of RGCs and rectangle behind circles represents boundaries of the electrode array (Field et al., 2007).

The RGCs are the only retinal cell type to send an axonal projection to the brain via the optic tract. The optic nerves are composed of the axons of the RGCs. The optic nerves from each eye come together at the optic chiasm. It is at the optic chiasm that RGC axons make the decision to cross the midline to project contralaterally or to stay on the same side to project ipsilaterally (Herrera et al., 2003; Williams et al., 2003). The proportion of contralateral to ipsilateral projections depends on the species. Binocular animals have equal proportions of contralateral and ipsilateral projections, while contralateral projections dominate in monocular animals. From the optic chiasm, RGC axons project to the target areas in the brain, such as the lateral geniculate nucleus, superior colliculus, and the non-image forming brain areas.

Physiological types of RGCs

Because the brain only receives signals from the RGCs, it is important to understand what sort of information the RGCs encode. Specific functions of RGCs

have been identified using different electrophysiological techniques, such as single-unit electrode recordings, calcium imaging, and multi-electrode arrays (MEAs). Like other neurons, RGCs have a baseline firing rate of action potentials, or spikes. RGCs respond to stimuli by changing the frequency of action potential generation. The change in spike rate, above baseline, represents the encoded information that is transmitted to the brain. By correlating the changes in spike rates to a well-defined visual stimulus, I can measure the functional properties of the RGCs. The following is a survey of different functional types of RGCs:

Some RGCs act as contrast detectors with antagonistic center and surround receptive fields (RFs). These properties were shown by experiments using intracellular recording electrodes while shining a spot of light or an annulus on the photoreceptors and determining the maximum response elicited (Kuffler, 1953). These experiments showed that RGCs have 3 basic responses to changes in contrast. ON-center, OFF-surround (ON) type RGCs respond to light onset in the center and light offset in the surround. OFF-center, ON-surround (OFF) type RGCs respond to light offset in the center and light onset in the surround. The third type of RGC is the ON-OFF type, which responds to both light onset and offset in its center. Importantly, anatomical features have been correlated to the ON/OFF responses. ON RGCs stratify their dendrites within the IPL closer to the GCL, while OFF RGCs stratify their dendrites within the IPL closer to the INL (Figure 6). ON-OFF RGCs stratify their dendrites in both regions of the IPL.

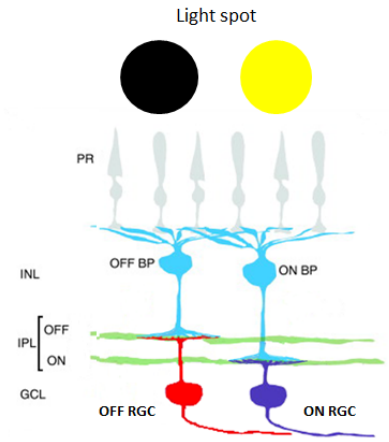

Figure 6. RGCs act as contrast detectors. The ON RGC (blue) responds to light onset (the yellow light spot) and contacts the processes of ON type bipolar cells in the sublamina of the IPL closest to the GCL. The OFF RGC (red) responds to light offset (the dark spot) and contacts the processes of OFF type bipolar cells in the sublamina of the IPL closest to the INL (adapted from Wei and Feller, 2011).

Contrast detector RGCs have been further classified beyond the ON/OFF distinction using other response properties. For example, RGCs can be classified as transient or sustained, depending on whether they fire a short burst of spikes or a more sustained spike train in response to a stimulus. Additionally, the size of the RF can be used to distinguish between RGCs. Smaller RFs have better spatial resolution, whereas larger RFs can cover more area to detect features. Since RGCs can respond to visual stimuli with varying time delays, the response latency is also a useful metric for RGC classification (brisk or sluggish).

Direction selective RGCs (DSRGCs), identified first in the rabbit retina, detect objects moving in a preferred direction, but respond less selectively to objects moving in different directions. 180° from the preferred direction is the null direction,

in which the DSRGC suppresses its response. Currently, 8 types of DSRGCs have been described. There are 4 types of ON-OFF DSRGCs, one for each of the four cardinal directions: nasal, temporal, dorsal and ventral (Figure 7). 3 types of ON DSRGCs have been described, which correlate with the orientation of the semi-circular canals in the inner ear that maintain balance (Barlow and Hill, 1963; Barlow and Levick, 1965; Oyster and Barlow, 1967). 1 type of OFF DSRGC has also been described (Kim et al., 2008). DSRGCs have been implicated in tracking objects and stabilizing images over the retina, as head and eye movements can distort the light projected on the retina.

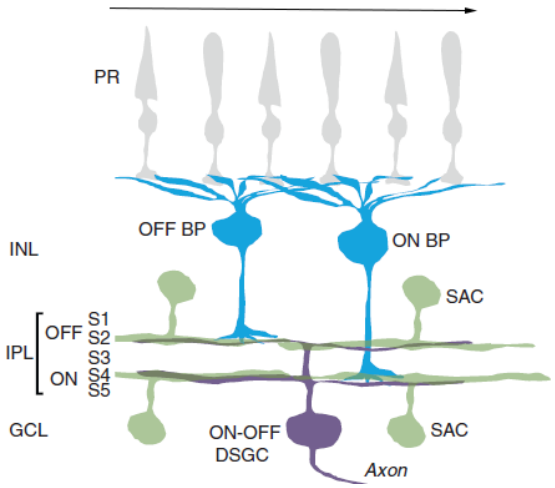

Figure 7. Direction selective RGCs respond to objects moving across the RF in a particular direction (arrow above the photoreceptors) (Wei and Feller, 2011). ON-OFF DSRGC makes synaptic connections with both the ON and OFF type bipolar cells as well as 4 starburst amacrine cells (SACs).

Non-image forming RGCs are involved in overall light detection but do not contribute to image forming visual processes. These RGCs are responsible for circadian entrainment and the pupillary light reflex (Berson, 2003). A subset of these,

the intrinsically photosensitive RGCs (ipRGCs) respond to light directly without photoreceptor input (Provencio et al., 2000). ipRGCs project to the non-image forming brain targets, such as the olivary pretectal nuclei and suprachiasmatic nuclei. ipRGCs typically respond to the onset of light of a specific wavelength in a sluggish and sustained fashion (Berson et al., 2002; Hattar et al., 2002; Guler et al., 2007; Chen et al., 2011).

The mouse retina

The mouse model offers several advantages in studying RGCs. Currently, direct links between morphology and function as scarce. This is because manipulating the morphology and determining the change in function cannot be performed in the more well-studied mammals. The mouse retina contains all the major retinal neurons and many of the same RGC types as primates and other mammals (Wassle and Boycott, 1991; Sun et al., 2002; Coombs et al., 2006; Berson, 2008; Volgyi et al., 2009). The mouse is also a convenient model organism, in that it has shorter gestation period (~28 days) compared to other mammals and fast visual system development (~24-30 postnatal days) (Huberman et al., 2008a). Importantly, the mouse offers the power of genetics, which is the most important consideration for choosing this model organism. Cell type identity and morphological features are specified in part by the genetic program of that cell type (Brown et al., 2001). By manipulating certain genes, such as cell adhesion molecules or transcription factors, the role of these genes in

retinal circuits can be characterized. Through this comparative genetic approach, anatomy, physiology and gene expression can be linked to create a better RGC classification system and to provide insight into RGC development.

Multielectrode array recording system

As mentioned, several approaches have been applied to functionally characterize the RGCs. Single-unit electrode recordings provide detailed information about single neurons, but do not allow for the study of population interactions (Shlens et al., 2006; Gauthier et al., 2009; Stafford et al., 2009). Calcium imaging can be used to analyze functional properties in populations of neurons, but lacks the temporal resolution needed to fully characterize response properties. Multielectrode arrays (MEAs) overcome these limitations; they are capable of recording extracellular electrical potentials from many neurons for long period of time in a single retinal preparation without loss of temporal resolution (Meister et al., 1994).

I choose to use a large-scale MEA system to record voltage changes from RGCs in the mouse retina (Litke et al., 2004). The MEA system was developed at the University of California, Santa Cruz by the Santa Cruz Institute of Particle Physics (SCIPP). Briefly, a piece of retina is isolated and perfused with oxygenated, physiological solution. The isolated retina can survive and respond to light for several hours. The retina is placed ganglion cell side down on the MEA and analog voltages are recorded. The array consists of 512 extracellular electrodes arranged in a

rectangle with a recording area of 1.7mm^2. By recording from numerous RGCs simultaneously, population features such as mosaic arrangement of RFs can be shown (Devries and Baylor, 1997; Chichilnisky and Kalmar, 2002; Field et al., 2007; Elstrott et al., 2008; Gauthier et al., 2009; Anishchenko et al., 2010; Sher and DeVries, 2012). Additionally, the MEA offers a quick approach to screen mutations in genes thought to be important in retinal function.

To analyze the high volume of data recorded by the MEA, the Vision software suite, developed by SCIPP, was used. Typically, 300-500 RGCs can be sampled in a single data run. This represents a significant advantage compared to single-unit electrode recordings (single neuron per data run) or low density MEA systems (tens of neurons per data run). However, with the increase in electrode density, the 512 MEA produces a large amount of data that needs to be analyzed. Vision software performs data analysis on these high volume datasets in a relatively short amount of time. Vision automates neuron identification, which distinguishes action potentials from individual neurons. Vision can also calculate spike triggered averages, which describes the average stimulus that elicits an action potential in an identified neuron.

Functional characterization of RGCs using MEA

Despite the wealth of information about different morphological and functional types, little is known about why these types are needed or how morphology relates to function. Using the large-scale MEA approach, my goal was to characterize

the functional properties of the RGCs in the wild-type mouse retina and see how these properties are perturbed in abnormal retinas. I first worked on a functional classification on the wild-type mouse RGCs. It was important to be able to see what response properties I could measure and what types of RGCs I could classify first in a normal retina. This would allow for a meaningful comparison to the mutant and transgenic retinas. I next utilized the data from the wild-type MEA recordings to describe anatomical and functional correlations in a mutant mouse line, the DSCAM knockout. This mouse line has a severe morphological defect in dendritic and cell body spacing. The DSCAM$^{-/-}$ mouse would allow me to see how manipulating the morphology could translate into functional differences. Finally, I used the MEA to characterize RGCs in the Isl2-DTA mouse line, in which a subset of RGCs was eliminated, to determine cell type identity. With a large subset of RGCs gone, I could determine and characterize the remaining types of RGCs. Eventually, I can find out which of the morphological types are missing and relate that to function. Overall my work will contribute to our understanding of what types of features in the visual scene are detected and how they may contribute to behavior.

Methods

Recording of retinal visual responses

Animals were cared for and used in accordance with guidelines of the U.S. Public Health Service Policy on Humane Care and Use of Laboratory Animals and the NIH Guide for the Care and Use of Laboratory Animals, and following institutional Association for Assessment and Accreditation of Laboratory Animal Care-approved practices. C57BL/6 wild-type mice were purchased from Charles Rivers Laboratories. *DSCAM*$^{-/-}$ mice, *DSCAM*$^{+/-}$, and *DSCAM*$^{+/+}$ littermates were provided by Dr. Peter Fuerst (Fuerst et al., 2010). An Isl2-flox-STOP-flox-DTA mouse line purchased from The Jackson Laboratory was crossed into a *CB2-Cre* line to generate Isl2-DTA; *CB2-Cre* mice, which will be referred to simply as Isl2-DTA. *CB2-Cre* mice express cre recombinase in a subset of RGCs in postmitotic neurons (ref). Genotypes of Isl2-DTA mice were confirmed by PCR using primers for Isl2-DTA (wild-type, 5'-GCCATGAGAACGCGGTGCAGGGC-3' and 5'-CGGAGTCTCCAGTCTCAGCGGTGC-3'; Isl2-fl-STOP-fl-DTA, 5'-ACGACGCTGCGGGATACTCT-3' and 5'-CAACGCTAGAACTCCCCTCA-3') and Cb2-Cre (wild-type, 5'-ACCTGGAGATTGTGCTCTGC-3' and 5'-GGGAAGCCAAAGAGAAAAGG-3'; CB2-Cre, 5'-ACCAGAGACGGAAATCCATCG-3' and 5'-TGCCACGACCAAGTGACAGCAATG-3'). Each mouse was dark-adapted for 20 minutes prior to anesthetization with a cocktail of 16 mg/mL ketamine (MWI

Veterinary Supply Company, Meridian, ID) and 4mg/mL xylazine (Sigma, St. Louis, MO) followed by cervical dislocation. Eyes were then enucleated under dim red light. The anterior of the eye and vitreous were removed and approximately 1x2 mm^2 piece of retina was peeled from the sclera and choroid. The retina was then placed on the 512 multielectrode array RGC side down and held in place by a 100µm pore size nylon mesh. The retina was perfused with a 30-32°C oxygenated bicarbonate buffered Ames' solution (Sigma, St. Louis, MO) and allowed to equilibrate for 30-60 minutes prior to the recording (Figure 8).

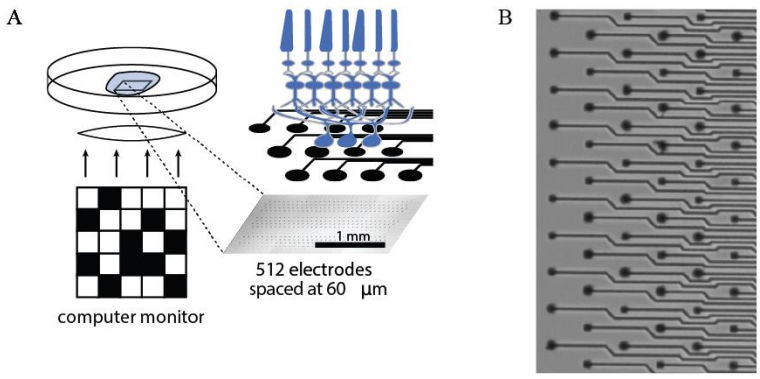

Figure 8. Large-scale MEA records action potentials from an isolated piece of retina. (A) The recording set-up involves placing an isolated piece of retina, RGC side down, on the rectangular, 512 electrode array. The array is designed to be in the base of a chamber to which Ames or physiological solution can be perfused. An image from a computer monitor is optically reduced by the microscope optics to project the image through the transparent electrode array and onto the photoreceptors. (B) A close up image of the electrodes is shown. Spacing between electrodes is 60µm. The entire array of has a recording area of 1.7mm^2.

Voltage traces from individual electrodes were digitized at a 20 kHz sampling rate and stored offline onto a hard drive for subsequent analysis to find spike times of individual RGCs (Litke et al., 2004). A few hundred RGCs were typically identified in a single retinal piece.

Visual stimulation

An optically reduced stimulus from a CRT monitor (Sony Trinitron Multiscan E100) was focused on the photoreceptors with the light passing through the transparent electrode array and the retina. RGC response properties were characterized through their spike triggered average (STA) response to a black and white binary spatiotemporal white noise visual stimulus (checker size: 80 μm; frame frequency: 60 Hz) (Chichilnisky, 2001). Each checker, termed a stimulation pixel or stixel, was 10x10 monitor pixels.

To measure the direction selective responses, full field drifting square waves were randomly presented in 16 different directions. Each direction was presented 5 times, each time for a duration 10 seconds followed by 3 seconds of gray screen (spatial frequency = 0.054 cycles/degree, drift frequency = 0.938 cycles/second) (Remtulla and Hallett, 1985).

Functional characterization of RGC responses to white noise stimulus

The voltage signal on each electrode during the white noise presentation was digitized at 20 kHz and stored for off-line analysis. Details of the recording and spike sorting methods are given elsewhere (Litke et al., 2004). STA responses to white noise stimulus were calculated for each of the identified RGCs. A two-dimensional Gaussian function was fitted to the spatial profile of each STA (Chichilnisky and Kalmar, 2002). The size of the RF was defined as the diameter of the circle with the area equivalent to that of the fitted Gaussian 1-sigma contour (Figure 9C). The electrophysiological image provides a dynamic image of each identified neuron (Figure 9D). The image is generated by averaging the analog waveforms across all electrodes on the MEA as a neuron fires an action potential (Litke et al., 2004; Sher and DeVries, 2012; Sher et al., 2013). The following steps were taken to select unique neurons with strong visual responses: (1) Cells with the less than 100 spikes were removed; (2) The cells with signal to noise ratio below 10 in their STA responses were removed; 3) The electrophysiological images of all identified neurons were compared to one another to remove duplicate cells. Typically, a few hundred unique RGCs per preparation were left after neuron cleaning.

Cell classification

Neurons were classified by grouping neurons with similar physiological responses (Devries and Baylor, 1997; Chichilnisky and Kalmar, 2002; Field et al.,

2007; Elstrott et al., 2008; Gauthier et al., 2009; Anishchenko et al., 2010; Sher and DeVries, 2012). The responses of the RGCs were characterized through their spike-triggered average (STA) response to a black and white flickering checkerboard, or white noise, visual stimulus (Figure 4A, checker size: 90µm x 90µm ; frame frequency: 60 Hz). For each identified RGC, the spatial sensitivity profile was characterized by iso-sensitivity contour. RGCs were classified as having ON- or OFF-set light sensitivity based on their STA time course (Litke et al., 2004). In particular, STA time courses, RF sizes and temporal autocorrelation functions (ACFs), also known as the inter-spike interval distribution, were used for classification (Figure 9). Individual cell types were not tracked across preparations due to a similarity between the types and variability from preparation to preparation. As a result of the classification process, the RGCs within each type had stereotypical STAs and ACFs that were different from cells classified in a different RGC type from the same preparation. Response latencies were calculated as the time to the first zero of the STA time course and the degree of transiency (DOT) was calculated as:

$$1 - \text{abs}(S)/S_{abs},$$

where S is the integral of the STA time course, and S_{abs} is the absolute value of the integral of the STA time course (Chichilnisky and Kalmar, 2002; Field et al., 2007). A value of 1 corresponds to transient responses, while a value of 0 corresponds to sustained responses.

Naming conventions differ from study to study. Here, the nomenclature of the functional classes was defined by the characteristics of the classification. The name of a class consists of 4 parts. First, an RGC can be ON or OFF type. Second, the RF diameter describes whether an RGC's RF was large, medium or small (L, M, or S). Third, the response latency describes the speed of the response to the onset of the stimulus, or more specifically, the time to zero. Two states were used: brisk or sluggish (B or S). Fourth, the RGC's transiency can be described whether it was a transient or sustained cell type (T or S). RGC classes were named relative to other classes in that particular recording.

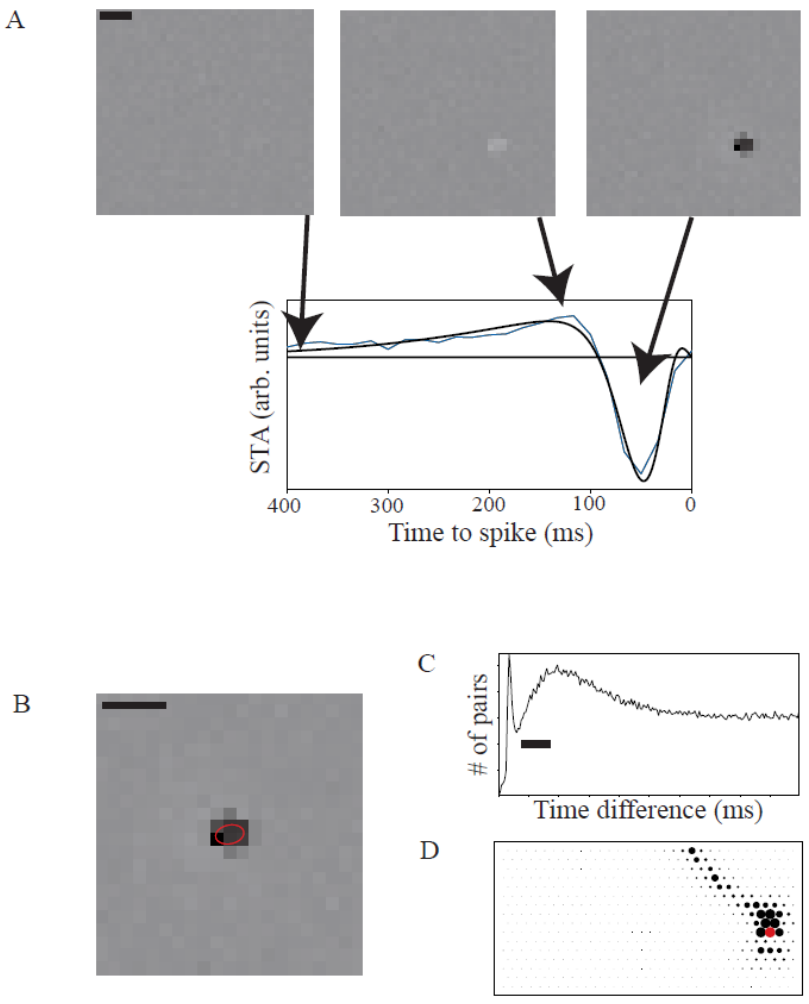

Figure 9. The STA for white noise describes the spatio-temporal response properties of an OFF type RGC. (A) The frames within 400ms prior to an action potential are stored. For every action potential in a recording, the frame sequences are averaged to produce a single sequence of frames within the 400ms time period to produce the STA. 3 frames from the STA are shown on top with arrows pointing to the time course of the STA on the bottom. Approximate time of frames: left = -400ms, middle = -118ms, right = -68ms. STA arb. unit 0 = gray, positive = lighter contrast, and negative = darker contrast. (B) The spatial RF is defined by the frame with an area with the most contrast difference, indicating the area the RGC was responsive to. 2D gaussian is drawn around the area of most contrast difference. Scale bar = 450µm. (C) The ACF is the interspike interval distribution. Scale bar = 10ms. (D) The EI of the RGC shows the average electrode activity across the MEA, revealing the position of the cell body and axon in reference to the electrodes.

Nearest neighbor distributions

The normalized nearest neighbor distances were calculated as described previously (Field et al., 2007). The distances were normalized according to RF radius in the direction of the nearest neighbor. The NNND between two cells is given by the following equation:

$$NNND = \frac{2R}{(\sigma_1 + \sigma_2)}$$

where R is the distance between the two RF centroids, and σ_1 and σ_2 are the SDs of the two Gaussian fits measured along the line connecting the two centroids. An NNND value of 2 signifies that the 1-sigma contours of the receptive field fits of two cells just touch each other without overlapping.

Density recovery profile

The density recovery profile was calculated as described previously (Rodieck, 1991).

Selection and functional characterization of direction selective RGCs

DSRGCs cells were identified and classified based on their responses to moving gratings. We did not analyze their receptive field spatial properties because STAs of ON-OFF DSRGCs were too noisy for such analysis, probably because most of them were ON-OFF DSRGCs. Direction selective responses were calculated by determining the number of spikes elicited during 5 presentations of 16 directions of the drifting square wave stimulus. The spikes rates were averaged over the 5 presentations, and normalized by dividing the individual spike rate at each orientation by the spike rates summed across all orientations. A cell's response to a direction was characterized by the vector with the length equal to this normalized response and the direction equal to the direction of the stimulus. Direction selectivity of a cell was then characterized by the vector sum of response vectors to all directions and called the direction selective vector of the cell (Figure 10). Its magnitude could vary from 0 (no direction preference) to 1 (responses to a single direction only). In addition, the Direction Selective Index (DSI) for each cell was calculated:

$$DSI = \frac{(pref - null)}{(pref + null)}$$

where *pref* is the average spike rate for the stimulus oriented closest to the direction selective vector, and *null* is the average spike rate for the stimulus 180 degrees away from *pref* (Elstrott et al., 2008). Cells with a DSI > 0.5 were classified as direction selective. Finally, the identified DSRGCs were required to have at least

100 spikes in response to the preferred direction, to ensure that high DSIs were not an artifact from spontaneous spikes.

To determine tuning curve width, the cell's responses were fitted to the von Mises distribution (Oesch et al., 2005):

$$R = R_{\max} e^{k\cos(x-m)} / e^{k}$$

where R is the average spike rate for motion in a given direction, x is the given direction in radians, R_{max} is the maximum response, μ is the preferred direction in radians, and k is the concentration parameter for the tuning width. All parameters were allowed to vary. Tuning curve width was then estimated as the full width at half height (fwhh) of the fitted curve (Elstrott et al., 2008):

$$fwhh = 2q$$

where,

$$q = arc\cos\left[\frac{\ln(0.5e^{k} + 0.5e^{-k})}{k}\right].$$

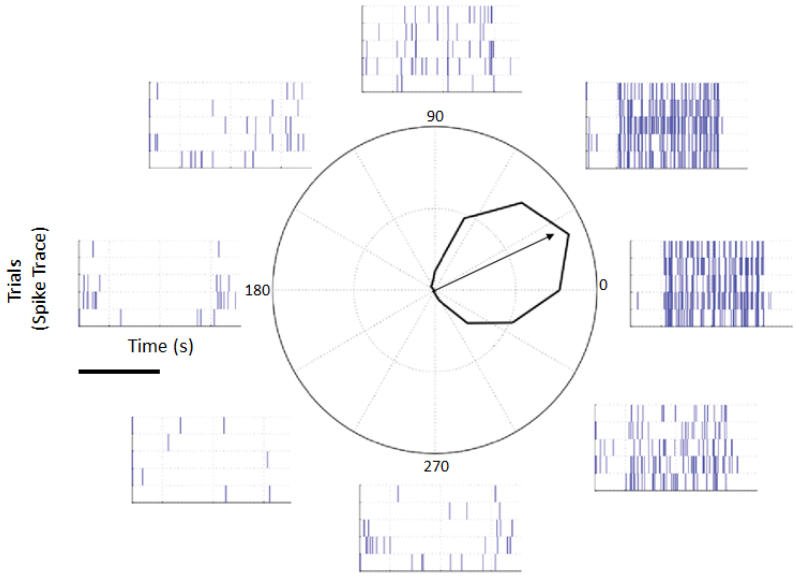

Figure 10. Direction selective retinal ganglion cells are identified by using a drifting square wave stimulus and shown on a polar plot. 16 different orientations are presented randomly 5 times during a stimulus run. Raster plots show the number of spikes that were elicited for 8 of the 16 directions presented, with each row representing 1 of the 5 presentations (trials), at that orientation. A vector is drawn on the polar plot with the direction reflecting the orientation of the bars and the magnitude representing the normalized response of the spike rate in that direction. Scale bar = 5s.

Immunohistochemistry

Adult (P30-60) eyes were enucleated and fixed in 4% paraformaldehyde for 1-2 hour. Retinas were dissected under a light microscope. Retinas were sunk in 30% sucrose overnight and then embedded in Tissue-Tek OCT compound (Sakura Finetek, USA Torrance, CA, USA) on dry ice. Cross sections of retinas were cut at 20µm sections on a CMI1520 Cryostat (Leica Microsystems, Buffalo Grove, IL, USA) at a temperature of -20°C and placed on glass slides. Sections were dried overnight at room temperature. Slides were then washed in 1X phosphate buffered saline (PBS),

then incubated for 1-2 hours at room temperature in blocking buffer (10% serum, 0.25% Triton x-100 in PBS). Sections were incubated with primary antibodies diluted in blocking buffer at the specified dilutions overnight at 4°C. The following primary antibodies were used: Brn3a goat polyclonal, 1:1000 (Santa Cruz Biotechnology, Santa Cruz, CA, USA); CART rabbit polyclonal 1:1000 (Phoenix Pharmaceuticals, Burlingame, CA, USA). The next day, sections were washed in 1X PBS and then incubated for 1 hour at room temperature with the appropriate fluorescently-conjugated secondary antibodies diluted at 1:1000 in blocking buffer. Slides were mounted with Fluoromount G (Southern Biotechnology, Birmingham, AL, USA). Sections with imaged with an Olympus 1X81 inverted confocal microscope (Olympus, Center Valley, USA).

Axon Tracing

Adult mice (P24-30) were anesthetized with 100/10 mg/kg ketamine (MWI Veterinary Supply Company, Meridian, ID) and xylazine (Sigma, St. Louis, MO) cocktail. Intraocular injections of CTB-555 in the left eye and CTB-488, both at 2 mg/mL, in the right eye were performed with a pulled glass capillary tube and a Picospritzer III (Parker Instruments, Carlsbad, CA, USA) set at 20 psi and 15ms pulses. Mice were allowed to recover for 5 days and then sacrificed, and perfused with 4% paraformaldehyde in PBS. Brains were dissected out of the head and fixed overnight at 4°C. The brains were washed in PBS, and then sunk in 30% sucrose at

4°C overnight. Coronal sections were cut 100µm thick with an HM430 sliding microtome (Thermo Fischer, Waltham, MA, USA). Sections were wet mounted onto glass slides with PBS. Sections with imaged with an Olympus BX51 epifluorescent microscope (Olympus, Center Valley, USA).

Chapter 1: Wild-type Mouse Retinal Ganglion Classification

Introduction

The retina is the neural tissue of the eye that extracts specific visual features from the environment that generates our perception of seeing. The retina utilizes parallel processing, in that these specific features are processed simultaneously and transmitted through separate, dedicated circuits. These circuits represent all of the features that the retina detects and sends to the brain. These circuits begin at the photoreceptors and end at the RGCs. Different types of RGCs define different circuits.

RGCs are a heterogeneous population, with each subtype being responsible for the detection a specific feature in the visual scene. Previous classification approaches have relied on clustering anatomical or physiological parameters into discrete groups. From these classifications, it is estimated that the mammalian retina contains more than 20 anatomically distinct RGC cell types and in excess of 12 physiological types (Dacey, 1999; Sun et al., 2002; Kong et al., 2005; Coombs et al., 2006; Berson, 2008; Volgyi et al., 2009; Farrow and Masland, 2011; Masland, 2012). However, it is not always the case that anatomy provides the clues to function, and it is currently not clear exactly how many functional classes of RGCs exist.

The mosaic principle, an organizational strategy within the 2D plane of a layer, is an indicator that a population of RGCs is a unique type of RGC. RGCs of the same type need to sample the entire visual field. In order to do so, they will space

their cell bodies out in a non-random, mosaic pattern across the retina while their dendrites tile the area in between the cell bodies (Wassle et al., 1981; Rodieck, 1991; Rodieck and Marshak, 1992; Dacey, 1993b). Functionally, mosaics have also been characterized. The spatial position of RFs within a class of RGCs will also have non-overlapping spacing (Devries and Baylor, 1997; Shlens et al., 2006; Field et al., 2007; Petrusca et al., 2007; Gauthier et al., 2009; Anishchenko et al., 2010; Sher and DeVries, 2012). Mosaics reduce spatial redundancy in signals between neighboring RGCs without introducing blind spots. Mosaics of different cell classes will overlap each other, allowing each circuit to fully sample the visual scene.

A large scale multielectrode array (MEA) approach has the capability to record from many different types of RGC within the same preparation (Devries and Baylor, 1997; Chichilnisky and Kalmar, 2002; Field et al., 2007; Elstrott et al., 2008; Gauthier et al., 2009; Anishchenko et al., 2010; Sher and DeVries, 2012). RGC population properties such as tiling arrangements of RFs can be measured with this approach. The MEA has been used to identify rare RGC types in the primate (Petrusca et al., 2007). MEAs record extracellular electrical potentials from many neurons for long period of time in a single retinal preparation, which allows several different stimuli runs to be performed enhancing cell type identification.

The mouse retina is an attractive model to perform RGC classification and circuit analysis due to the ease of genetic manipulation. By manipulating the genetics, morphological features can be altered and functional changes can be measured thus

providing direct links between form and function. A functional RGC classification in the wild-type mouse retina will provide a good reference when recording from genetically modified retinas, where certain circuits are perturbed. Future studies will then show what genes are required for particular circuits, thus linking genetics to function.

Here, a large-scale MEA was used to measure the response properties of hundreds of RGCs simultaneously in the wild-type mouse retina. Spatio-temporal white noise and drifting square waves were used as stimuli to drive responses in RGCs. Reverse correlation was used to determine the average stimulus that elicited a response (Chichilnisky, 2001; Elstrott et al., 2008). Using the white noise stimulus, RGCs could be split into ON and OFF populations. Upon further classification, 2 ON types and 2 OFF types were found most often in preparations. Other RGC classes can be detected but less frequently than these transient types. Classes were validated by the mosaic principle, in which RFs in an individual class are arranged in mosaics across the visual field. Using the drifting square waves to stimulate direction selective RGCs (DSRGCs), 4 DSRGCs were found, though the reliability of finding all four directions in one preparation was variable. Together, the results from the wild-type mouse RGC functional classification show 4 contrast detectors and 4 DSRGCs can be detected and used for further analysis of genetically manipulated retinas.

Results

White Noise Classification

To measure the spatio-temporal response properties of RGCs, white noise stimulus, a flickering checker board of black and white squares, was projected onto the retina. This stimulus was used to sample the centers of RGC RFs in order to determine the spatial extent of the center, the response kinetics and the degree of transiency. After neuron identification, the spike triggered average (STA) can be calculated and assigned to each identified neuron. The features of the STA were used as classification criteria. In order to begin classification, the first step is to remove the neurons that do not have good signal to noise ratios in the STA. The next step is to remove duplicate neurons based on the similarities between their electrophysiological images (EI). The remaining neurons are those with good signal to noise and these are the ones used for classification.

18 C57BL/6 wild-type mouse retinas were recorded. The neuron identification procedure in Vision software found on average 576 ± 34 neurons per retina. The remove weak time courses indicated that on average, 170 ± 25 neurons were considered to have weak signal to noise. Duplicate removal indicated that on average, 91 ± 13 neurons were considered duplicates based on the EI.

RGCs were grouped together based on similarities in the time course of the STA, RF diameter, and the temporal ACF (see Methods). Principal components analysis is performed on the STA time course and ACF. Each principal component is

plotted on a 2D Cartesian plane in combination with another principal component (PC) or the RF diameter with each neuron represented by a single point (Figure 11C). Clusters represent neurons that have similar properties with one another along the 2 dimensions. The first notable clusters along the first time course component represent the ON and OFF types (Figure 11A-C). When classified in this way, the resulting overlay of all the contours of the RF in one class was arranged in mosaics. Within the 18 C57BL/6 recordings, 139 ± 14 ON type RGCs and 175 ± 14 OFF type RGCs on average were classified.

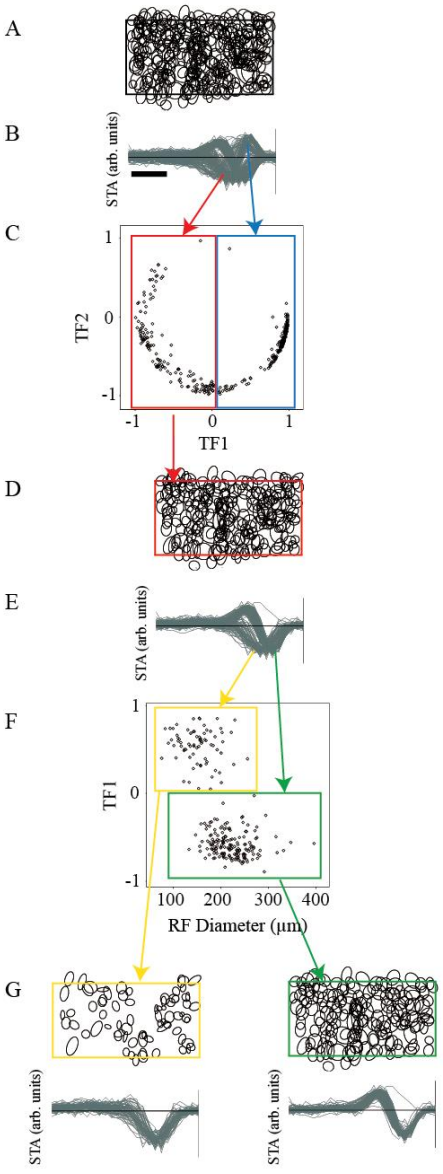
A
B
STA (arb. units)
C
TF2
1
0
-1
-1
0
1
TF1
D
E
STA (arb. units)
F
TF1
1
0
-1
100
200
300
400
RF Diameter (µm)
G
STA (arb. units)
STA (arb. units)

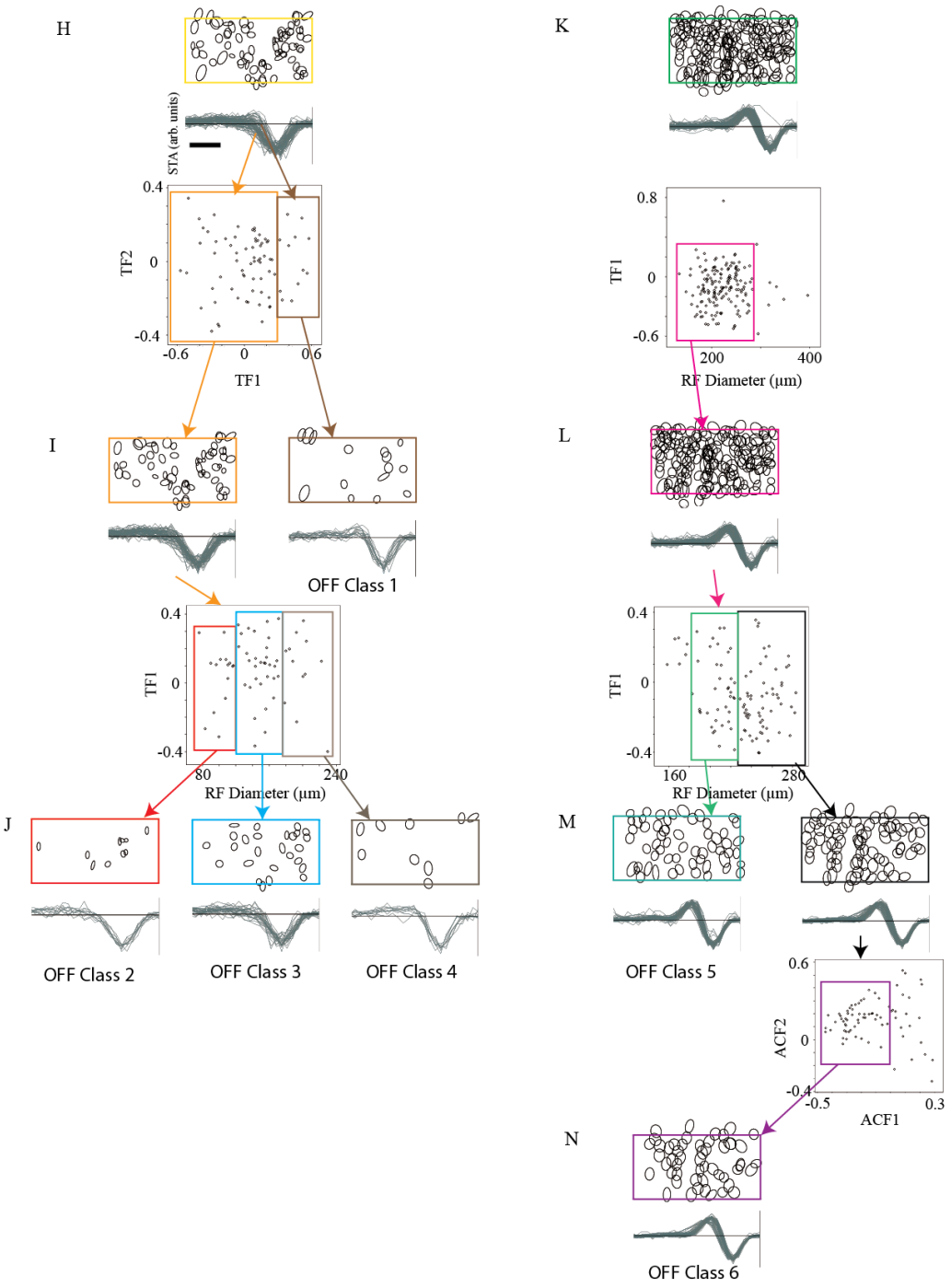

Figure 11. White noise classification is performed by grouping together RGCs with spatio-temporal response properties. (A) The overlay of all RGC RFs (ellipses) identified in a single recording shows extensive overlap prior to classification. (B) The overlay of the time courses of the STA shows two major peaks which represent the ON (blue) and OFF (red) classes. (C) Principal components analysis performed on

the time course and the first 2 components (TF1 and TF2) are plotted against each other. Along the first component, two clusters are seen that correspond to the two major ON and OFF peak in the time course. (D) Classification of the OFF type RGCs from A-C. RF overlay of all OFF type RGCs are shown. (E) The overlay of the time courses for all OFF types. (F) The first principal component of the time course vs. the RF diameter is used to separate the OFFs into two groups (G), a sluggish, sustained type (left) and a brisk, transient type (right). (H-J) Sustained OFF types are classified. (K-N) Transient OFF types are classified. Classification for the ON type RGCs are done in the same way..

The ON and OFF classes can then be divided according to other features. Typically, more sustained classes can be separated from more transient classes. Also, slower response latency classes can be separated from faster response latency classes. The RF diameter is also used to divide neuron into large, medium and small classes. Recordings did show variability from preparation to preparation. However, the RF diameter ranged from 57-211μm. The range of time to zero, which is one measure of response latency, was 87ms to 243ms. The degree of transiency ranged from 0.96 to 0.34, with 1.0 being the most transient and 0 being the most sustained. Both ON and OFF type RGC classes fell into two broad categories based on their time to zero and degree of transiency: the brisk, transient classes and the sluggish, sustained classes.

From the 18 recordings made, I was able to classify about 4-8 RGC types for each recording. However, 4 RGC types could be found with the most consistency and had relatively complete mosaic arrangement of RFs across all recordings. These are all transient types of RGCs that fire an initial, transient burst of action potentials upon stimulus onset. These types also have larger RF diameters. These are termed the large, brisk transient and medium brisk transient RGCs. The smaller, more sluggish

RGC classes were more difficult to find and mosaics were not complete in most cases (Figure 12). The next sections describe the 4 most common RGC classes in the C57BL/6 recordings using white noise stimulus.

OFF Large Brisk Transient

At least one class in each recording was designated as OFF LBT. This class featured an average RF diameter of 154µm ± 4µm, an average time to zero of 119.2ms ± 3.8ms, and an average degree of transiency of 0.88 ± 0.01. This class typically had the most complete RF mosaic relative to the other types and was found in all 18 recordings.

OFF Medium Brisk Transient

The OFF MBT shared very similar response properties to the OFF LBT class, but had smaller RF diameters and separate mosaics. The OFF MBT class featured an average RF diameter of 130µm ± 4µm, an average time to zero of 117.3ms ± 3.8ms, and an average degree of transiency of 0.80 ± 0.02. Each of the 18 recordings had an OFF MBT class.

ON Large Brisk Transient

The ON LBT class was the most common of the ON classes. The ON LBT class featured an average RF diameter of 159µm ± 5µm, an average time to zero of 116.8ms ± 4.8, and an average degree of transiency of 0.81 ± 0.02. 16/18 recordings had an ON LBT class.

ON Medium Brisk Transient

The ON MBT shares similar characteristics with the ON LBT class, but had smaller RF diameters and separate mosaics. The ON MBT class featured an average RF diameter of 123µm ± 8µm, an average time to zero of 127.4ms ± 4.4ms, and an average degree of transiency of 0.80 ± 0.03. The ON MBT class appeared in 11/18 of the recordings.

Sluggish, Sustained Cell Types

Sluggish and sustained cell types were also identified, but were not present in all recordings. The small, sluggish, sustained RGC classes were better represented in the 18 recordings than larger RF diameter sluggish, sustained classes. These classes rarely formed complete mosaics, unlike the LBT and MBT classes described previously.

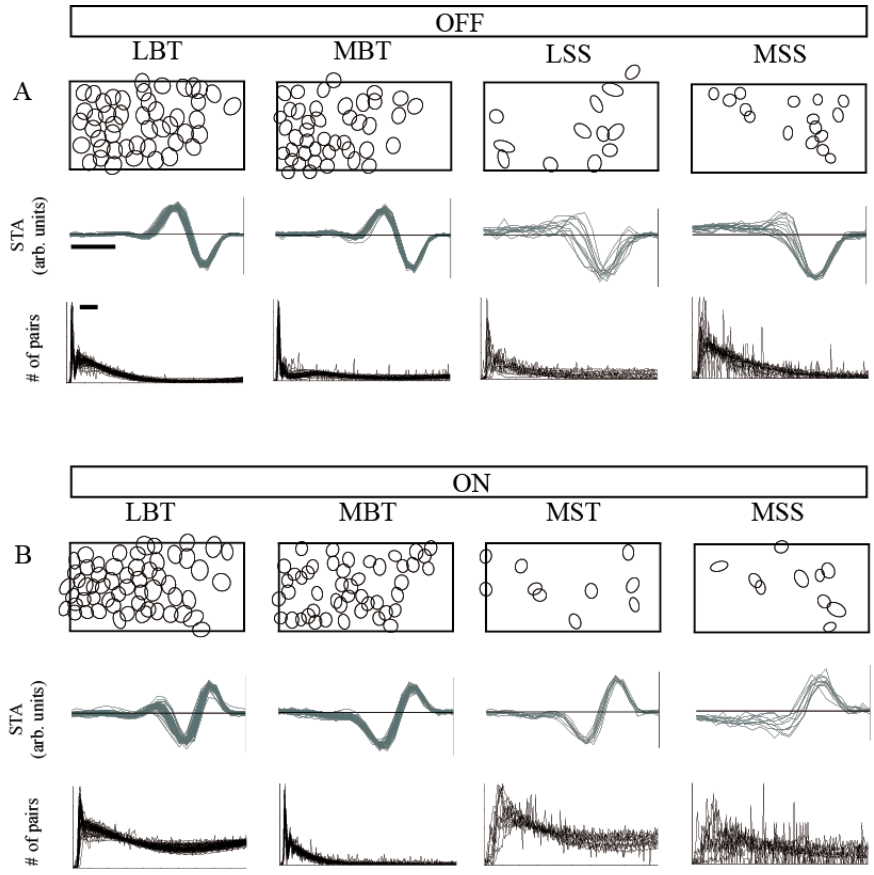

Figure 12. White noise analysis in one retinal preparation on the MEA allows for the functional classification of RGCs. (A) Four OFF classes and (B) four ON classes were identified. For each class, the RF mosaic (top), STA time course (middle) and temporal autocorrelation (bottom) are shown. Each ellipse or trace in a plot represents functional properties from a single RGC. Mosaic box = 1.7mm2. Time course scale bar = 100ms. Autocorrelation scale bar = 10ms. LBT = large brisk transient, MBT = medium brisk transient, LSS = large sluggish sustained, MSS = medium sluggish sustained, MST = medium sluggish transient.

Direction Selective Retinal Ganglion Cells

The DSRGCs were identified using drifting square wave stimuli. DSRGCs were identified as having a DSI over 0.5 (Elstrott et al. 2008) and vectors representing individual neurons were plotted on polar plots. Detection of DSRGCs was highly variable across preparations. Some recordings identified up to 4 directions (Figure 13), while other recordings had less than 4 directions and some recordings even had very few total DSRGCs.

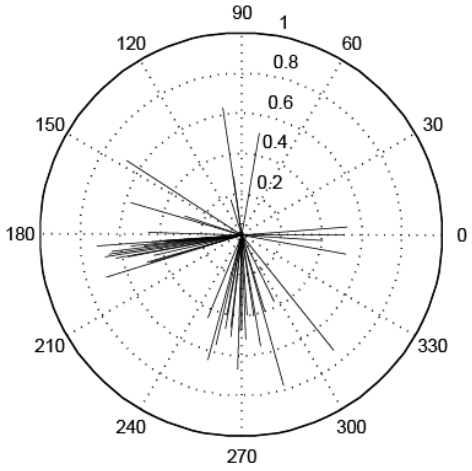

Figure 13. DSRGCs from one retinal preparation show responses to 4 different directions. Vectors showing the preferred direction and magnitude of the response representing the DSRGCs are shown on a polar plot. The 4 directions are separated by 90°.

Discussion

Here, I describe a method for functionally classifying wild-type mouse RGCs. Such a classification is necessary to understand the types of visual channels in the

retina. The classification reliably identified 2 OFF type and 2 ON type contrast detectors, while 4 types of DSRGC could sometimes be detected. The OFF LBT type was the most common of all cell classes and was used as a reference for naming other cell classes within the retina. This RGC class often consisted of the most complete RF mosaic. The OFF LBT may be the functional correlate of the OFF transient αRGCs, a subtype that can be labeled with SMI-32, a marker of neurofilament. αRGCs were first identified in the cat retina, but have been found across mammals (Boycott and Wassle, 1974; Peichl et al., 1987; Peichl, 1991; Pang et al., 2003; Huberman et al., 2008b). They have large cell bodies and dendritic fields consistent with the large RF diameters characteristic of the OFF LBT class. The response properties of the OFF LBT are also consistent with that of the αRGCs, having brisk and transient responses to light stimuli (Fukuda et al., 1984). It is harder to speculate on the morphological correlates of the OFF MBT, ON LBT and ON MBT classes. Because RF size correlates with dendritic field size, these cell classes should have medium to large dendritic fields that are monostratified in the appropriate OFF or ON sublamina of the IPL (Berson, 2008). The 4 types of DSRGCs may correspond to the ON-OFF DSRGCs that have been described as responding to the 4 cardinal directions: dorsal, temporal, ventral, and nasal (Barlow and Hill, 1963; Barlow and Levick, 1965; Oyster and Barlow, 1967).

Currently, this classification obtained through large-scale MEA is not complete, but can be improved. The sluggish, sustained types were not detected consistently. Also, the smaller cell types were not detected as consistently as the

larger cell types. In order to improve RGC class detection, improvements or entirely new stimuli can be employed. The white noise or direction selective stimuli optimally stimulated certain classes, but not others. One advantage of the MEA approach is that the extracellular electrodes do not penetrate into the RGCs and the lifespan of the retina in vitro can last longer than 6 hours. This allows for the presentation of different stimuli within the same preparation. Although the white noise parameters are optimal for detection of the most common cell types, checker size and refresh rate can be changed, leading to the detection of other RGC classes. Additionally, local direction selective stimuli can be used to sample individual directionally selective receptive fields. Circular spots that contain moving bars inside of them can be projected randomly in space similar to how white noise samples RFs. Other RGC types require specific stimuli. For example, the intrinsically photosensitive, melanopsin RGCs (ipRGCs) respond to blue light and have very slow, sustained time courses (Berson et al., 2002; Hattar et al., 2002). In combination with these changes in the visual stimuli, denser electrodes can also be employed. A different electrode array containing 519 electrodes, with 30μm electrode spacing has already been developed. The small recording area is the main drawback to this particular array, but can supplement the classifications obtained with the 512 MEA approach.

Despite not being a complete classification, the 8 RGC classes described provide a basic framework for visual circuits in future studies. RGC fate determination is controlled in part by activity independent mechanisms (Erkman et al., 1996; Brown et al., 2001; Shirasaki and Pfaff, 2002; Elstrott et al., 2008; Badea et

al., 2009; Anishchenko et al., 2010). Currently, few molecular markers of RGC have been characterized, which is a limitation of studying individual types of RGCs (Pak et al., 2004; Huberman et al., 2008b; Kim et al., 2008; Huberman et al., 2009; Kay et al., 2011; Osterhout et al., 2011; Sweeney et al., 2014; Triplett et al., 2014). By recording from retinas in which certain genes are knocked out, circuits and RGC functional properties in mutant retinas can be compared to the wild-type retina. This will lead to identification of genes that are required for development of particular features and contribute to the discovery of RGC molecular markers.

Mosaic arrangement of RFs in an RGC class is a conserved feature across retinas. (Devries and Baylor, 1997; Shlens et al., 2006; Field et al., 2007; Petrusca et al., 2007; Gauthier et al., 2009; Anishchenko et al., 2010; Sher and DeVries, 2012). An MEA approach is essential in identifying mosaic arrangements, as many RGCs need to be recorded in order to show neighbor-neighbor spatial relationships of RFs. Classifications were not performed using mosaic principle as criteria. Instead, the STA time course, RF diameter, and the temporal ACF were the only criteria used to classify RGCs, and RF mosaics were the result of these methods. Mosaics were used after classifications to confirm that RGCs grouped together were indeed individual classes. The organization of the RFs of an RGC class seems to follow that of the anatomical spacing of the RGCs across the 2D GCL. This suggests that the developmental program that establishes the anatomical spacing will have a direct effect on the spatial positioning of the RF. Testing this hypothesis is possible as a DSCAM KO mouse is available, in which same type RGC cell bodies and dendrites

clump independently of other types (Fuerst et al., 2008; Fuerst et al., 2009; Fuerst et al., 2010). By recording from DSCAM KO retinas and comparing RF mosaics with wild-type retinas, structure and function correlates can be made directly.

The 512 MEA approach has the capability of recording the electrical activity from hundreds of neurons and it remains a possibility that all RGC types can be detected in a single preparation. By increasing the number of RGC types that can be detected, more circuits can be analyzed in more detail. The addition of new stimuli and the modification of current stimuli parameters will enable more RGC types to be detected. This will be important for the analysis of mutant retinas or perturbed circuits. The MEA approach presents a quick and easy method to screen such retinas. An understanding of the functional aspects of the retinal circuits will enable new and more effective treatments for visual defects.

Chapter 2: DSCAM is required for mosaic arrangement of receptive fields and direction selective responses in mouse RGCs

Introduction

The retina performs a wide range of visual processing through parallel circuits, each consisting of specific types of retinal neurons connected in a distinct way. At the output of each circuit is a distinct type of RGC (Dacey, 2004; Wassle, 2004; Coombs et al., 2006; Berson, 2008). Each RGC type forms a non-random, independent, spatial mosaic that can be observed anatomically by the regular spacing between cell bodies and a steady degree of overlap between dendritic arbors (Wassle et al., 1981; Rodieck and Marshak, 1992; Dacey, 1993a) and physiologically, by the tiling of the receptive fields (RFs) of RGCs of the same type (Devries and Baylor, 1997; Field et al., 2007; Petrusca et al., 2007; Gauthier et al., 2009; Anishchenko et al., 2010; Sher and DeVries, 2012). The most obvious role of this orderly arrangement is ensuring that individual parallel retinal pathways sample the visual field in a uniform way. However, until recently it was not possible to directly test what role the mosaic-like anatomical arrangement of retinal neurons plays in determining encoding properties of the retina. In this paper we use mice lacking the Down Syndrome Cell Adhesion Molecule (DSCAM) (Millard et al., 2007; Fuerst et al., 2008; Clandinin and Feldheim, 2009; Blank et al., 2011; Matsuoka et al., 2011) to answer this question.

DSCAM is required for the formation of the anatomical mosaics of some retinal cell types. In *DSCAM*$^{2j/2j}$ mutant mice (hereafter referred to as *DSCAM*$^{-/-}$) the regular spacing of cell somas of dopaminergic, bNOS positive, and cholinergic amacrine cells as well as SMI-32 and melanopsin expressing RGCs, is disrupted. In addition, the dendrites of these neurons tend to fasciculate, resulting in uneven coverage of the retinal area (Fuerst et al., 2009; Fuerst et al., 2010). DSCAM is expressed widely throughout the RGC layer and it is suggested that all types of RGCs require DSCAM for self-avoidance (Fuerst et al., 2008). Electroretinogram responses in *DSCAM*$^{-/-}$ retinas indicate light responsiveness and functional synapses do not require DSCAM (Fuerst et al., 2009). In this study we aimed to determine how the anatomical abnormalities affect functional response properties of the distinct retinal pathways by comparing the RGC responses to visual stimulation between wild-type and *DSCAM*$^{-/-}$ retinas.

Using a large-scale MEA to record the extracellular electrical activity from hundreds of RGCs simultaneously, we find that DSCAM is required for the formation of direction selective circuits but not ON and OFF circuits. ON and OFF RGC types showed slightly slower response properties and more elongated receptive fields in *DSCAM*$^{-/-}$ retinas. Unlike those in wild type retina, receptive fields of individual RGC types do not form mosaics in DSCAM mutant retina, demonstrating the DSCAM is essential for the generation or maintenance of receptive field tiling. These results show that the orderly anatomical arrangement of retinal neurons is required for the

normal retinal function at the neural population (regular spatial sampling) and individual neuron (temporal filtering and direction selective responses) levels.

Results

We characterized retinal functional properties by recording the responses of RGCs to a spatio-temporal white noise and moving gratings stimulation using the 512 multielectrode array. Cells that had spike triggered-average responses to the white noise stimulus with signal-to-noise ratio > 5 were classified according their STA responses and autocorrelation functions in each preparation (7 wild-type, 4 *DSCAM*$^{+/-}$, 8 *DSCAM*$^{-/-}$ retinas). Direction selective RGCs (DSRGCs) were selected based on their responses to square-wave gratings moving in different direction.

The response latency of individual RGCs is slower in DSCAM mutant.

Fasciculation of RGC dendrites and amacrine cells' dendritic and cell bodies arrangement in *DSCAM*$^{-/-}$ retina can lead to changes in receptive field size and shape as well as in temporal response properties of individual RGCs. To test this hypothesis we compared average receptive filed size as well as response latency and degree of transiency for two broad categories of RGC types: brisk-transient and sluggish-sustained. The two categories were separated based on the response latency and the degree of response transiency (Figure 14A) and consisted of multiple functional RGC

types across multiple preparations. Variability of functional properties of individual RGC types between preparations did not allow us to perform a more detailed classification. We found that for the brisk-transient cell types there was no significant change in receptive field size and response transiency between wild-type and *DSCAM*$^{-/-}$ (Figure 14B, D), but the response latency was slightly but significantly slower for the *DSCAM*$^{-/-}$ (Figure 14C). Consistent with this, there were more sluggish-sustained cell types detected in the *DSCAM*$^{-/-}$ retinas and they had slower response latency that that of the wild-type and *DSCAM*$^{+/-}$ ones (Figure 14A). Note that we do not calculate the averages for the sluggish-sustained cells because of their wide and uneven distributions over both response latencies and transiency. Thus, at the level of individual spatio-temporal receptive fields, the main effect of the DSCAM deletion is increase in the RGC response latency, but the spatial receptive fields are not affected at the resolution of our stimulus (100 μm). The increase in RGC response latency could reflect altered synaptic connectivity in the *DSCAM*$^{-/-}$ retina due to the clumping of RGC dendrites and amacrine cells' dendritic and cell body arrangement.

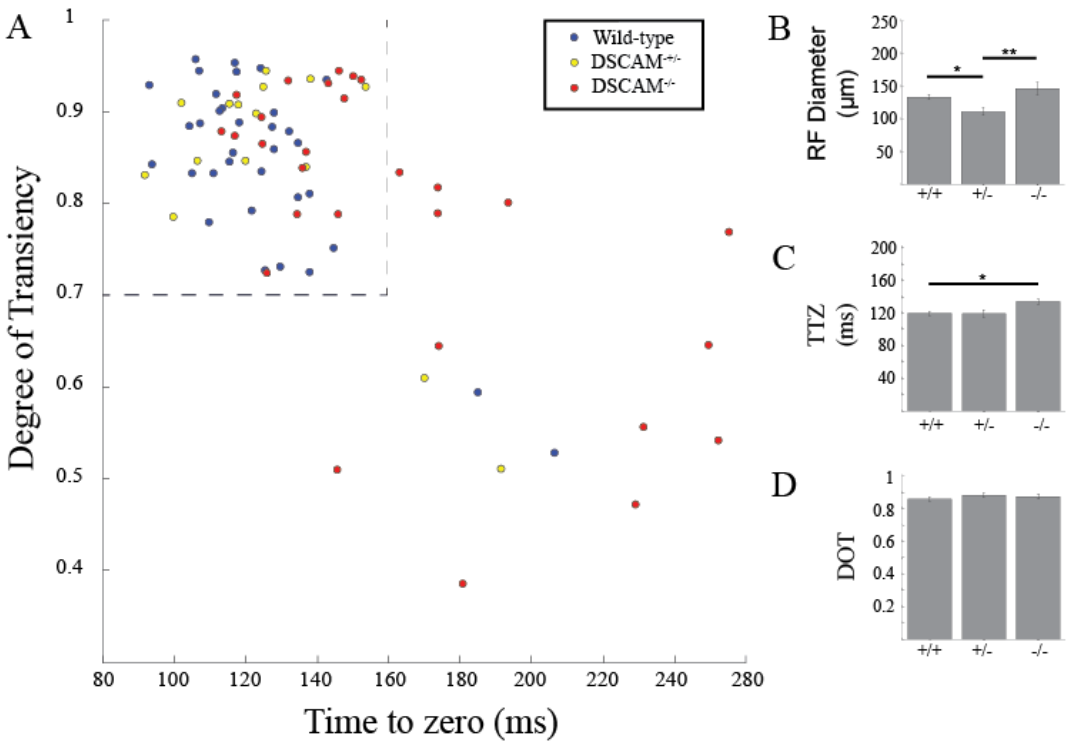

Figure 14. *DSCAM*$^{-/-}$ RGCs maintain basic response properties to white noise stimulus, although have slower time to zero responses. (A) Scatter plot of time to zero vs. degree of transiency of all RGC classes from all 7 wild-type, 4 *DSCAM*$^{+/-}$ and 8 *DSCAM*$^{-/-}$ retinas. Each circle represents an individual RGC class, where blue is wild-type, yellow is *DSCAM*$^{+/-}$, and red is *DSCAM*$^{-/-}$. The dotted boundary represents the brisk, transient RGC classes which were used for further analysis in B-D. (B) Bar graphs compare the average RF diameter between the genotypes. Differences were observed between WILD-TYPE and *DSCAM*$^{+/-}$, and between *DSCAM*$^{+/-}$ and *DSCAM*$^{-/-}$. (C) Bar graphs compare the average time to zero of the three genotypes. Differences were observed between wild-type and *DSCAM*$^{-/-}$ classes. (D) Bar graphs compare the average degree of transiency. No significant differences were observed between genotypes. Two-tailed T-test were used to test for significance between the genotypes where * indicates < 0.05 and ** indicates < 0.001.

Non-random tiling of the visual space by receptive fields of the individual wild-type RGC types.

Due to the defects in the spacing of cell bodies and dendritic arbors of DSCAM mutants, the tiling of RFs within individual RGC types can be disturbed. In order to test this hypothesis we first characterized RF tiling in wild-type retinas. We observed that the receptive fields of the classified RGC types tiled visual field in a non-random manner with minimal overlap and with neighboring RFs just touching each other (Figure 15A). This observation was confirmed by the normalized nearest neighbor distribution having no entries at or close to 0 and peaking around 2 (Figure 15D). This is the first observation of the orderly visual space tiling by the receptive fields of individual RGC types in the mouse and is consistent with previous results in the rabbit, macaque monkey, and rat retinas (Shlens et al., 2006; Field et al., 2007; Petrusca et al., 2007; Gauthier et al., 2009; Anishchenko et al., 2010). Note that the apparent gaps in the RF mosaics are due to the RGC detection and identification inefficiencies as well as the strict selection criteria (see Methods).

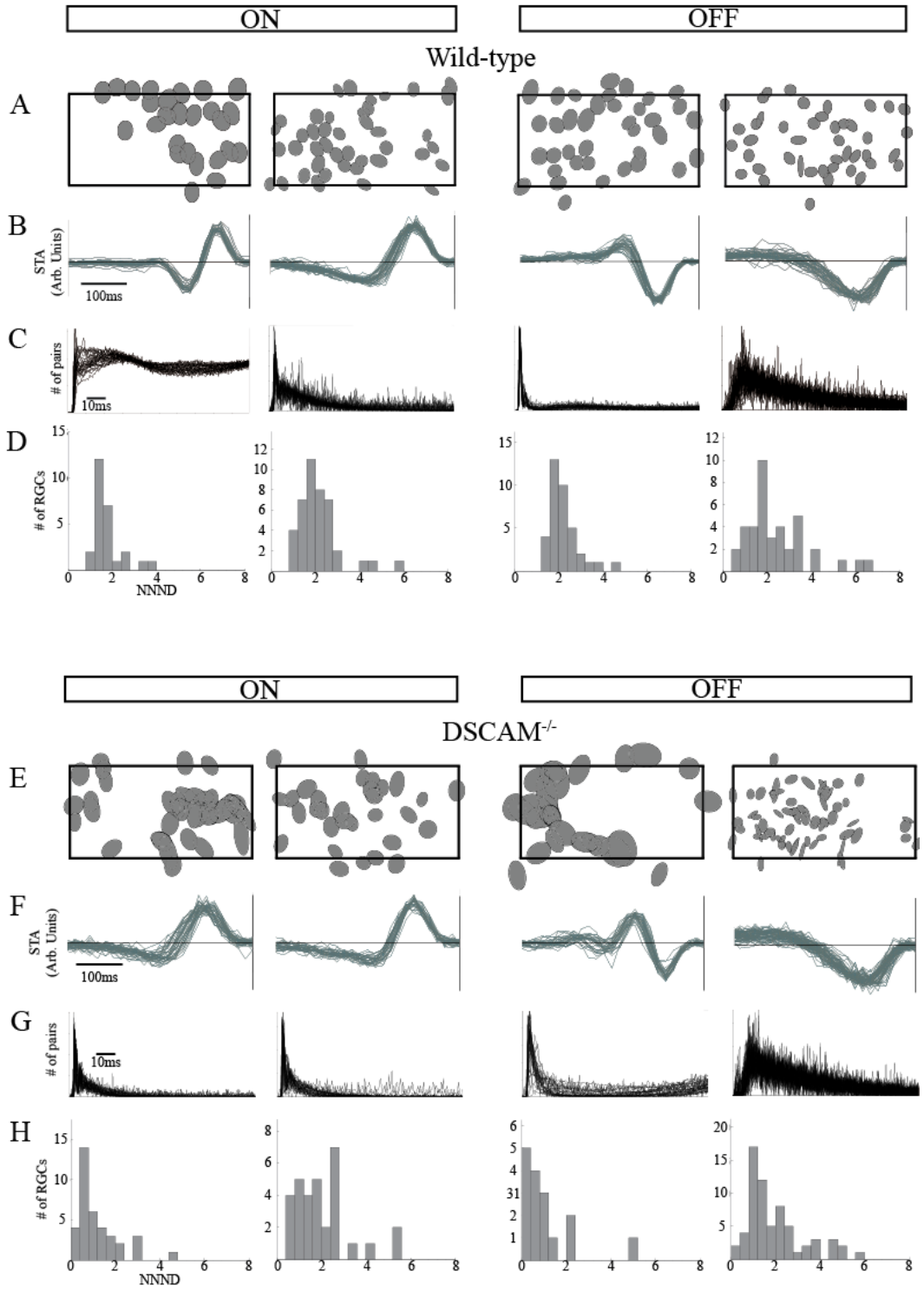

Figure 15. RFs in individual *DSCAM*$^{-/-}$ RGC classes exhibit clumping phenotype. (A) Examples of RF maps of ON and OFF wild-type RGC classes. RFs of each class tile

the visual field by touching just at the boundaries of the Gaussian fits. The rectangle represents the edge electrodes of the MEA and has an area of 1.7mm^2. (B) Time courses of the STA and (C) the temporal autocorrelation function for wild-type and heterozygote classes shown above in A. Each RGC in a cell class shares similar time course and autocorrelation traces which were used as parameters, along with RF diameter, for classification. (D) Normalized nearest neighbor distribution of the cell classes in A. A value of 2 signifies RFs touching just at their edges (see Methods). Most NNNDs for wild-type and *DSCAM*$^{+/-}$ classes are centered near 2. (E) Examples of RF maps of ON and OFF *DSCAM*$^{-/-}$ RGC classes. RFs in each class identified displayed a higher degree of overlap than wild-type or *DSCAM*$^{+/-}$ classes. (F) Time courses of the STA, (G) temporal autocorrelation function and (H) NNND of *DSCAM*$^{-/-}$ RGC classes. NNNDs of *DSCAM*$^{-/-}$ RGC classes were shifted to shorter distances.

Tiling arrangement of RFs of individual RGC types are disrupted in the DSCAM$^{-/-}$ *retinas*

DSCAM$^{-/-}$ RGCs were classified in the same way as the wild-type ones. However, the RFs within individual RGC types showed apparent overlap absent in the wild-type (Figure 15E). This observation was confirmed by the NNND distributions (Figure 15H): the whole distribution shifted to the left with the dip at smaller distances observed for the wild-type either reduced or completely eliminated.

In order to distinguish between regular tiling, random placement, and clustering of the receptive fields we calculated the density recovery profile (DRP) (Rodieck, 1991) of the centers of the RFs of the RGCs within each functional type. The center location of each receptive field was defined as the center of the 2D Gaussian fitted to the STA (see Methods). The regular tiling results in the DRP exclusion zone (density within an average RF diameter is small or zero), random

placing corresponds to the flat DRP profile, and clustering would result in an increased density at small distances. Only RGC types with more than 20 cells or 25% coverage of the MEA area were considered for DRP analysis. As expected, we found a DRP exclusion zone for the wild-type RGCs, which was either absent or significantly reduced in DSCAM$^{-/-}$ retinas (Figure 16A). We quantified this difference by extracting average density within an average RF diameter (inner density) and outside (outer density) of that radius (Figure 16A) from each calculated DRP (Figure 16A). The cross-plot of these two densities for all of the detected RGC types confirms regular tiling (inner density < outer density) for the wild-type and DSCAM$^{+/-}$ RGC types, while the DSCAM$^{-/-}$ RGC types showed spatial arrangement that was more consistent with either random placing or even clustering where the probability for the receptive fields to overlap was higher than that predicted by random placing (Figure 16B).

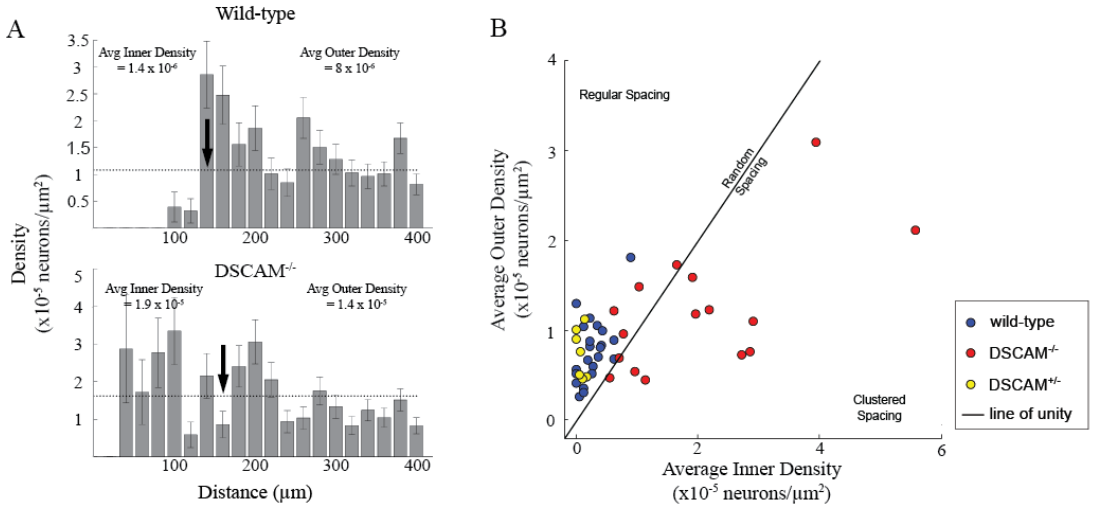

Figure 16. DRP summary quantifies the clustering of *DSCAM*$^{-/-}$ RFs compared to the regular spacing of wild-type RFs. (A) Example DRP of a wild-type and *DSCAM*$^{-/-}$ RGC class. Arrows indicate the average RF diameter of each class (130µm for wild-type and 160µm for *DSCAM*$^{-/-}$). Dotted line represents random spacing of the RFs. A large exclusion zone at the smaller bins is characteristic of wild-type cell classes due to regular spacing of RFs. RFs of RGCs in wild-type classes do not encounter another RF of the same RGC class until distances close or beyond the average RF diameter. RFs of RGCs in *DSCAM*$^{-/-}$ classes have high densities at distances closer than the average RF diameter, suggesting clumping or random arrangements. Average inner density is the average of the densities at bins from 0 µm to RF diameter of that class. Average outer density is the average of the densities at bins from the RF diameter to 400 µm. (B) Cross plot of the average outer density vs. the average inner density. Blue points represent 22 wild-type cell classes, yellow points represent 7 *DSCAM*$^{+/-}$ cell classes, and red points represent 16 *DSCAM*$^{-/-}$ cell classes. Classes with large exclusion zones, and are spaced regularly, exhibit larger average outer densities compared to average inner densities. Classes with a random spatial organization of RFs have equal average inner and outer densities and fall on the line of unity. Classes with RFs that cluster have larger average inner densities.

DSCAM$^{-/-}$ *retina has fewer and weaker Direction Selective RGCs*

We next tested if DSCAM is required for the development of direction-selective circuitry of the retina. DSRGCs were identified based on the responses to gratings moving in different directions (see Methods). Four wild-type DSRGC types

with four approximately orthogonal preferred directions (Oyster and Barlow, 1967) were identified (Figure 17A), consistent with them being ON-OFF DSRGCs. However, the fraction of DSRGCs was on average 10 times lower in the *DSCAM*$^{-/-}$ retinas ($p = 1.2x10^{-3}$, single-value Kolmogorov–Smirnov test; Figure 16C). Furthermore, we found that the few identified *DSCAM*$^{-/-}$ DSRGCs had lower direction selectivity ($p = 2.7x10^{-12}$, t-test; Figure 17D) and broader tuning curve ($p = 2.7x10^{-12}$, t-test; Figure 17A, B, E) than those measured in wild-type DSRGCs. To test if the DSRGCs are still present in the *DSCAM*$^{-/-}$ mice we stained wild-type and *DSCAM*$^{-/-}$ retinas with CART antibody that was shown to label DSRGCs (Kay et al., 2011). We did not observe an obvious lack of CART staining in the *DSCAM*$^{-/-}$ retinas (Figure 17F-I). These results indicate that the lack of direction selective responses in the *DSCAM*$^{-/-}$ retina is caused by abnormal synaptic connectivity rather than the absence of DSRGCs themselves.

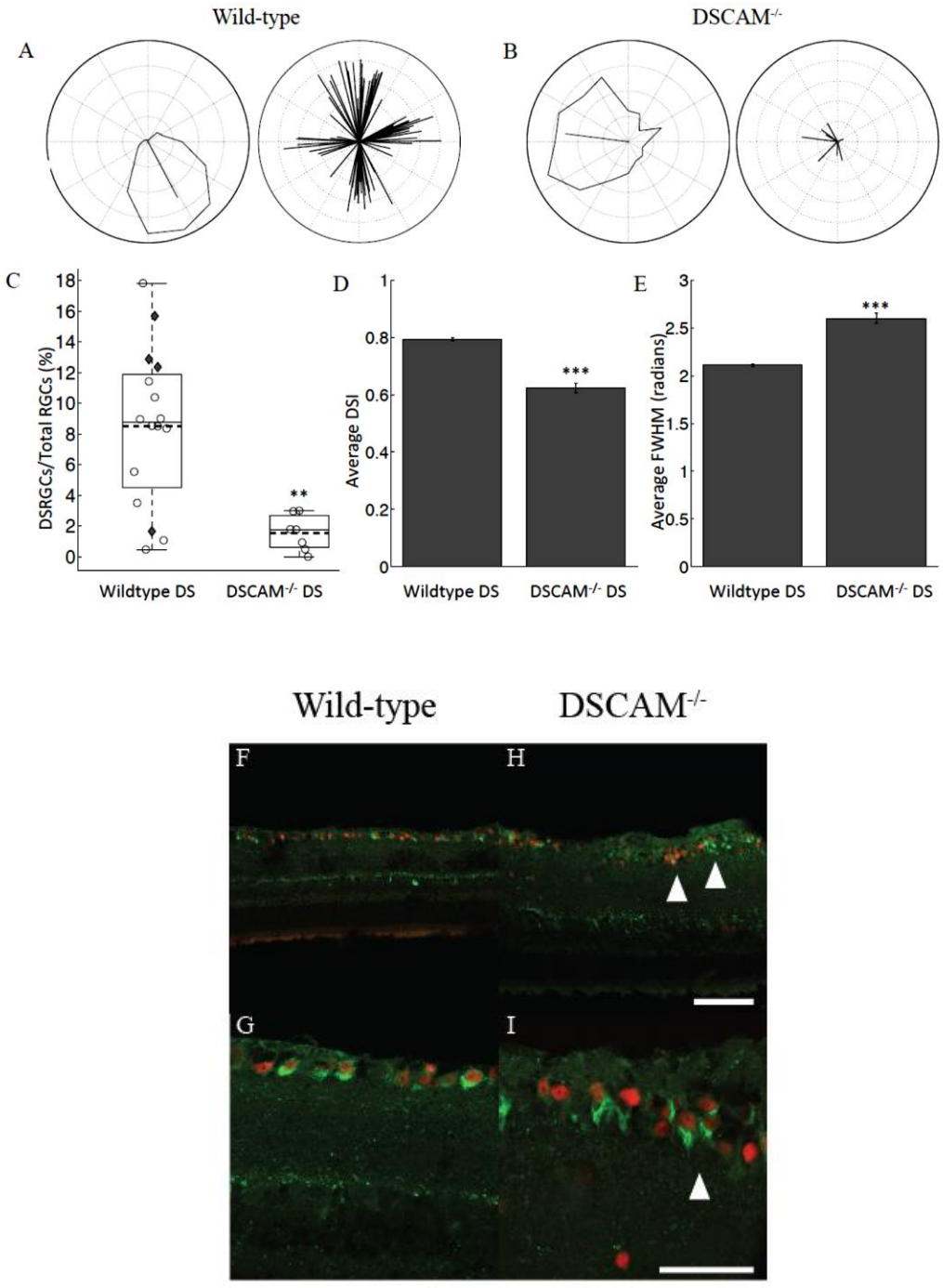

Figure 17. *DSCAM*$^{-/-}$ retinas contain fewer DSRGCs compared to wild-type. (A and B) The left polar plots show the tuning curve of the spike rate (spikes/sec) of a single DSRGC. Normalized spike rates were vector summed to produce a Direction Selective vector for each neuron. The right polar plots show the Direction Selective vectors for all DSRGCs in one wild-type retina (A) and one *DSCAM*$^{-/-}$ retina (B). (C)

Boxplot showing the percentage of RGCs that are DSRGCs for each retina. Points indicate individual retinas, with circles indicating mutant or wild-type, and grey diamonds indicate *DSCAM*$^{+/-}$. The center line indicates the median, the dotted line indicates the average, the box edges indicate the 25th and 75th percentiles, and the whiskers indicate the most extreme data points, ($p = 1.2x10\text{-}3$, Kolmogorov–Smirnov test) (D) Bar graph showing the average DSI for DSRGCs in wild-type and *DSCAM*$^{-/-}$. Error bars are SEM, ($p = 2.7x10\text{-}12$, t-test). (E) Bar graph showing the average full width at half maximum (FWHM) for DSGCs in wild-type and *DSCAM*$^{-/-}$. Error bars are SEM ($p = 2.5x10\text{-}17$, t-test). **p<0.01, ***p<0.001. Immunohistochemistry performed on cross sections of wild-type (F-G) and *DSCAM*$^{-/-}$ (H-I) retinas. Green labels CART positive RGC and red labels Brn3a positive RGCs. (F) Wild-type Brn3a and CART positive RGCs are arranged in a single layer, with higher magnification in (G). (H) Brn3a and CART positive RGCs in the *DSCAM*$^{-/-}$ section is disorganized, with higher magnification in (I). (F and H) Scale bar = 100µm. (G and I) Scale bar = 50µm. Arrowheads indicate clumps of RGCs.

Discussion

Within the retina, neurons are organized both vertically and horizontally. Cell bodies and synaptic connections are arranged in different layers. Individual cell types, such as individual RGC types, are arranged in nonrandom mosaics across the 2D plane of the layer. This spatial arrangement is thought to be important for the uniform sampling of the visual space, but the functional consequences of disturbing the orderly mosaic of RGC cell bodies and their dendrites have never been tested. Here we took advantage of the *DSCAM*$^{-/-}$ retina, which exhibits anatomical defects in cell body, dendritic positioning and synaptic lamination, to determine the effects of a well-defined anatomical phenotype on the function of retinal circuits. To do so, we recorded the response properties and RF locations of many RGCs in wild-type and *DSCAM*$^{-/-}$ retinas using a large-scale MEA.

Distinct functional pathways are preserved in the DSCAM$^{-/-}$ retina

Distinct functional properties of the parallel retinal pathways arise from selective connectivity between specific photoreceptor, bipolar, amacrine, and ganglion cell types. One possible consequence of the inner plexiform layer disruption observed in the *DSCAM*$^{-/-}$ retinas (Fuerst et al., 2010; de Andrade et al., 2014) is that this precise connectivity is disturbed resulting in the absence of distinct functional RGC types. However, we found that we are able to classify *DSCAM*$^{-/-}$ RGCs into functional RGC types based on their spatial and temporal filtering properties indicating that selective retinal connections are retained despite the spatial defects in the *DSCAM*$^{-/-}$ retina.

Functional properties of non-direction selective retinal pathways are largely normal

We found no significant differences in the average receptive field sizes of the *DSCAM*$^{-/-}$ non-direction selective RGC types and transiency of their responses when compared to the wild-type RGCs. It is however possible that a higher resolution measurement of spatial sensitivity profile of *DSCAM*$^{-/-}$ RGCs would reveal some disturbance in their receptive field organization caused by the dendrite fasciculation. Finally, we measured a small increase (15ms) in the average RGC response latency in the *DSCAM*$^{-/-}$ RGCs. This increase might be caused by disturbed synaptic connectivity. Previous studies show that functional connectivity between rod and rod bipolar cells in mice that lack a related cell adhesion molecule, DSCAML1, is

immature (Fuerst et al., 2009). However no similar studies were performed for cone connectivity. Spatial disturbance of RGC, amacrine and bipolar cell processes in IPL can also contribute to the increased response latency through disorganization of synapses. All-in-all, it is not surprising that the temporal filtering is affected in the *DSCAM*$^{-/-}$ retina, but this change most likely has multiple sources that are yet to be determined.

Direction selective RGCs are mostly absent in DSCAM$^{-/-}$ *retina*

We found that the direction selective circuitry is severely compromised in DSCAM mutant retinas. *DSCAM*$^{-/-}$ retinas had far fewer DSRGCs than those from wild-type. Even those RGCs that were identified as DSRGCs in the *DSCAM*$^{-/-}$ retina had weaker direction selectivity. The retinal circuitry that creates DS responses is more complex than that of non-DS circuits, and some DS circuits rely on the asymmetric synapse formation of starburst amacrine cells with DSRGCs (Trenholm et al., 2011). The starburst amacrine cells provide inhibition when the DSRGCs are presented with a bar moving in the null direction, but allow for the DSRGCs to be excited when presented stimuli in the preferred direction (Wei and Feller, 2011). Due to massive RGC dendritic fasciculation in the absence of DSCAM, DSRGCs may not be able to connect to the starburst amacrine cells in a spatial manner that establishes preferred and null directions properly. Furthermore, ChAT bands in the inner plexiform layer, which represent the processes of starburst amacrine cells, are

disrupted in the DSCAM$^{-/-}$ retina (Fuerst et al., 2010; Schramm et al., 2012; de Andrade et al., 2014). Since starburst amacrine cells do not express DSCAM, the defect in ChAT band organization in the *DSCAM*$^{-/-}$ retina is likely a secondary effect of the processes of these cells having to locate synaptic sites on the highly fasciculated dendrites of the RGCs. This would lead to both lamination defects and improper establishment of symmetrical connections between the two cell types resulting in weaker DS responses in RGCs. Alternative explanation of the scarcity of the direction selective responses in the *DSCAM*$^{-/-}$ retina could be that the DSRGCs are absent. We did not observe an obvious lack of CART staining in the *DSCAM*$^{-/-}$ retinas, indicating that DSRGCS are still present, and it is indeed the disturbance of retinal neural circuitry that leads to the absence of the direction selective responses.

Clumping of RGC cell bodies leads to the disturbance of the regular functional sampling of visual field

We observed that while the RFs within a single functional RGC type tile visual field in a regular manner in the wild-type retina, this well-known organization is severely disturbed in the *DSCAM*$^{-/-}$ retina. This finding shows that the hallmark uniform sampling of visual field by the individual RGCs relies mostly on the regular RGC spacing and local interactions between receptive fields of neighboring RGCs are not strong enough to counteract the RGC cell body displacement (Gauthier et al., 2009). We found that the RF placement within an individual RGC type was most

frequently consistent with clumping rather than random placement confirming the anatomical phenotype.

In conclusion we show that the regular anatomical mosaics formed by the cell bodies and dendritic arbors of the retinal neurons serve multiple purposes in functional organization of the retina. On the individual RGC level, for non-direction selective pathways their disturbance in the *DSCAM*$^{-/-}$ retina has little effect, but the direction-selective pathways are obliterated almost completely. On the population level, uniform sampling of visual field is severely disturbed by the defects in regular spacing of RGC cell bodies. These findings are for the first time directly proving the importance of spatial organization of neural circuitry in the retina.

Chapter 3: Characterization of RGCs after genetic ablation of Islet2 RGCs using Diphtheria Toxin

Introduction

Over 20 different types of RGC have been described using anatomical and physiological criteria, suggesting many different pathways and feature detectors. (Dacey, 1999; Sun et al., 2002; Kong et al., 2005; Coombs et al., 2006; Berson, 2008; Volgyi et al., 2009; Farrow and Masland, 2011; Masland, 2012). In chapter 1, I used the 512 MEA to characterize and classify RGCs by their functional properties. An understanding of the functional properties of the RGCs is crucial to determining what features the retina extracts and how those features relate to visual perception and behavior.

The development of different RGC types depends on gene expression (Erkman et al., 1996; Brown et al., 2001; Shirasaki and Pfaff, 2002). A retinal progenitor will divide and differentiate into all the different types of RGCs. The generation of RGC diversity requires differential expression of transcription factors. Efforts have been made to identify transcription factors expressed in subsets of RGCs (Badea et al., 2009; Sweeney et al., 2014; Triplett et al., 2014). However, it is not yet known what the transcriptional codes are for every RGC type.

Islet2 (Isl2) is a LIM homeodomain transcription factor found in approximately 40% of all RGCs. Isl2 is expressed specifically by contralaterally projection RGCs, while ipsilaterally projecting RGCs do not express it (Pak et al.,

2004; Triplett et al., 2014). This suggests that Isl2 plays a role in determining laterality of RGC projections in the optic chiasm. An Isl2-GFP line indicated that the SMI-32 population of RGCs, which specify a subset of RGCs including the alpha RGCs, overlaps with Isl2 (Boycott and Wassle, 1974; Peichl et al., 1987; Peichl, 1991; Pang et al., 2003; Huberman et al., 2008b). Additionally, an Isl2-GFP mouse line showed RGCs projecting to brain targets involved in image forming vision, the dorsal lateral geniculate nucleus (dLGN) and the superior colliculus (SC), but not to non-image forming targets (Triplett et al., 2014). Therefore, Isl2 expressing RGCs may not be involved in non-image forming visual processes. However, the specific cell types and functional properties of RGCs that express Isl2 are not yet known.

Here, RGC function, molecular identity and brain projections are characterized in a mouse line that lacks Isl2 RGCs. These RGCs were eliminated by genetic activation of DTA (Diphtheria Toxin A) in an Isl2-DTA mouse line. DTA inhibits protein synthesis causing cells that express it to die, while sparing the cells that do not express it (Maxwell et al., 1987; Chen et al., 2011; Zhang et al., 2012). DTA was specifically expressed in RGCs by crossing the Isl2-DTA mouse line, which contains a floxed stop codon, to a *CB2-Cre* line, in which Cre recombinase is expressed behind the *Calbindin-2* promoter. It is expected that ipsilateral RGCs should be spared, as well as some of the contralateral projections. RGC death was confirmed by the reduced optic nerve diameter. SMI-32 and Brn3a, molecular markers of RGCs, were both reduced in immunohistochemistry experiments, further proving cell death occurred. Using a large scale MEA approach to record response

properties of the remaining RGCs, Isl2-DTA retinas contained significantly reduced numbers OFF type RGCs. RGC projections to the contralateral dLGN were reduced, while the ipsilateral projections seemed normal. Surprisingly, the ipsilateral inputs to the dLGN did not appear to expand their territory in the absence of the contralateral inputs. The contralateral and ipsilateral projections to the SCN of Isl2-DTA animals were unaffected. These results show that Isl2 specifies a specific subset of RGCs that include OFF types that project contralaterally to brain targets involved in image formation. This work will ultimately lead to how individual retinal pathways contribute to behavior.

Results

Islet2-DTA mice have thin optic nerves

To investigate what types of RGCs Isl2 specifies, Isl2 expressing RGCs were ablated using DTA. A conditional mouse line that expresses DTA behind the Isl2 promoter was generated using a Cre-lox system. Isl2-DTA mice were viable, exhibited no motor function defects, and could breed, suggesting that most body systems were unaffected. P30-P60 mice were used in experiments, a point when the visual system is fully developed (Huberman et al., 2008a). Isl2-DTA mice were compared to littermate controls for all experiments. Littermate controls have the Isl2-DTA allele but do not express Cre. The diameter of the optic nerve was reduced resulting in a thinner nerve fiber in the Isl2-DTA mice compared to litter mate

controls (Figure 18A). The optic nerve is composed of the axons of the RGCs. A reduction in optic nerve diameter is a good indicator of RGC loss. Mice containing only one DTA allele exhibited thin optic nerves suggesting that expression of any DTA was lethal. These results show that RGC axons were eliminated due to the expression of DTA.

Reduced SMI-32 and Brn3a labeled RGCs in Isl2-DTA retinas

To determine if RGC cell bodies were indeed eliminated in the retina, whole mount retinas were prepared and immunohistochemistry was performed with markers of RGCs to visualized cell bodies. Brn3a is a transcription factor that is expressed in approximately 80% of all RGCs (Quina et al., 2005; Badea et al., 2009). Brn3a immunostaining labels RGC cell bodies, which are densely labeled across littermate control retinas. This is in contrast to the Brn3a staining in the Isl2-DTA retina, where very few RGCs are labeled (Figure 18B). This indicates that not only are RGC axons eliminated, but their cell bodies are also eliminated. This also indicates multiple cell classes are most likely eliminated as Brn3a is expressed in several different types of RGCs (Badea and Nathans, 2011).

SMI-32 positive RGCs are also reduced in Isl2-DTA retinas. SMI-32 is a marker of neurofilament and labels a subset of RGCs that include the alpha RGCs (Peichl, 1991; Huberman et al., 2008b; Bleckert et al., 2014). Compared to littermate control retinas, SMI-32 staining is reduced in the Isl2-DTA retinas (Figure 18C). This

indicates that α RGCs maybe one type of RGC that is eliminated in the Isl2-DTA retina.

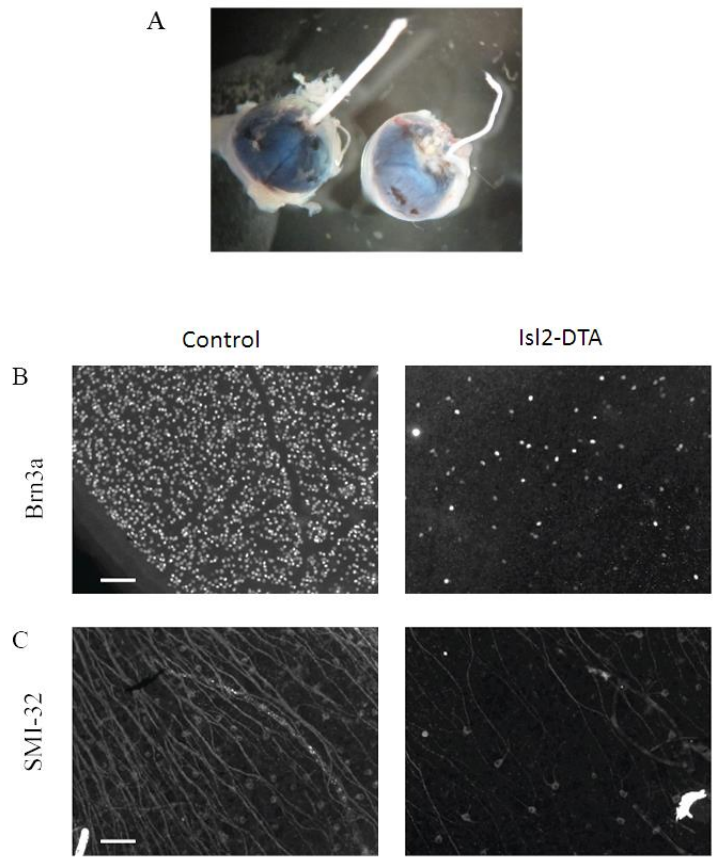

Figure 18. Genetic activation of DTA results in RGC death. (A) The enucleated eye with optic nerve in the Isl2-DTA mouse (right) is shown in comparison to the optic nerve of a littermate control (left). (B,C) Immunohistochemistry was performed on whole mount retinas. Brn3a RGCs are labeled in B. SMI-32 RGCs are labeled in C. Scale bar for B and C = 100µm.

Functional characterization of Isl2-DTA retinas

Isl2 could be a subset of RGCs that all have similar response properties and prefer particular stimuli, or cell death may be unspecific with loss of all types. In

order to determine which functional types of RGCs remain in the Isl2-DTA retina, the large scale MEA was used to record the response properties of Isl2-DTA retinas to white noise stimulus. 4 Isl2-DTA retinas and 2 control littermates were recorded. Isl2-DTA retinas were light responsive and recorded activity from RGCs produced STAs indicating that some visual channels still remain. Neuron identification detected more total neurons prior to neuron cleaning, which involves removing neurons with bad signal to noise ratios and duplicates, in controls than Isl2-DTA retinas (861± 102 average neurons, n = 2 for control and 538 ± 45, n = 4 for Isl2-DTA recordings). After neuron cleaning, an average of 338 neurons could be used for classifications in controls and 153 neurons were used for classifications in Isl2-DTA ($p = 0.02$, t-test). The percentage of clean neurons out of the total per preparation was similar between the littermate control and Isl2-DTA retinas (39.2% in controls vs. 30.2% in Isl2-DTA retinas, $p = 0.2$, t-test). These data show that there was a decrease in the number of RGCs that were detected in Isl2-DTA retinas. The decrease in number of RGCs detected was the result of cell death and not due to an increase in the number of noisy or duplicate neurons found in Isl2-DTA preparations.

Notably, the number of OFF type RGCs was significantly reduced in the Isl2-DTA mice compared to littermate controls (Figure 19 and 20). In Isl2-DTA recordings, ON type RGCs account on average 90% of all clean neurons and OFFs for 10%. In littermate controls, the ON types account on average 51.4%, while OFFs account for 48.6% of all clean neurons. In C57BL/6 recordings from Chapter 1, OFF type RGCs slightly outnumbered ON type RGCs. ON types account on average

44.4%, while OFFs account for 55.6% of all the clean neurons in C57BL/6 recordings. The average number of ONs per Isl2-DTA prep was 139 ± 30 RGCs, while the average number of ONs per littermate control prep was 174 ± 28 RGCs. The average number of OFFs per Isl2-DTA prep was 14 ± 4 RGCs, while the average was 164 ± 16 RGCs in controls (Figure 21). Within the 18 C57BL/6 recordings in Chapter 1, 139 ± 14 ON type RGCs and 175 ± 14 OFF type RGCs were classified. The number of ON type RGCs in the Isl2-DTA preparations was comparable to typical wild-type recordings despite the reduction in total RGCs detected in those retinas. This finding suggests that Isl2 is expressed specifically in OFF type RGCs and that cell death was not random, but restricted to these OFF type RGCs.

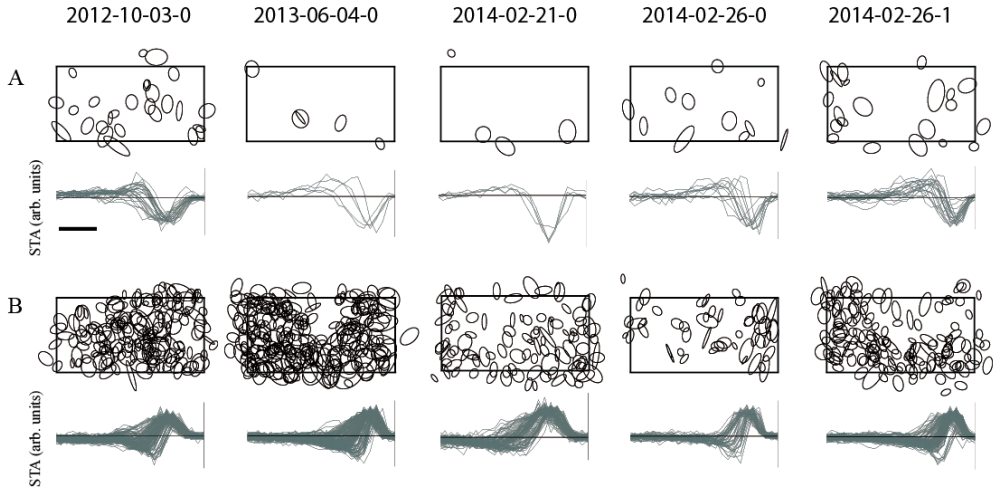

Figure 19**.** Less OFF type RGCs are found in Isl2-DTA retinas in response to white noise stimulus. (A) All OFF RGCs found across 5 Isl2-DTA retinas. Each date represents a single retina. Overlays of RFs (top) and STA time courses (bottom) are shown for each preparation. (B) All ON RGCs found across the same 5 Isl2-DTA retinas as in A. Overlays of RFs (top) and STA time courses (bottom) are shown for

each preparation. Box represents the recording area of the MEA and is 1.7mm^2. Scale bar = 100ms.

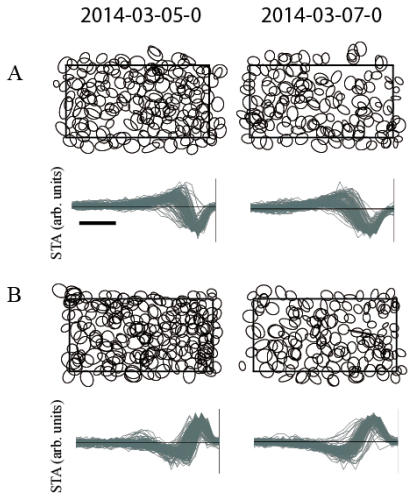

Figure 20. The normal compliment of OFF type RGCs are found in Isl2-DTA littermate control retinas in response to white noise stimulus. (A) All OFF RGCs found across 5 control retinas. Each date represents a single retina. Overlays of RFs (top) and STA time courses (bottom) are shown for each preparation. (B) All ON RGCs found across the same 5 Isl2-DTA retinas as in A. Overlays of RFs (top) and STA time courses (bottom) are shown for each preparation. Box represents the recording area of the MEA and is 1.7mm^2. Scale bar = 100ms.

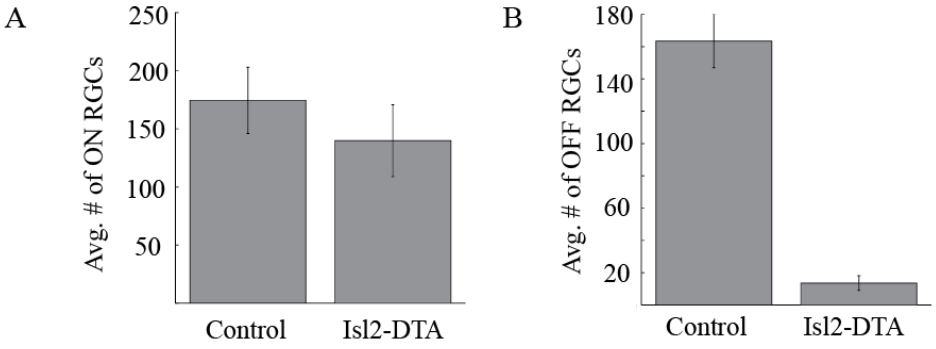

Figure 21. The average number of OFF is reduced in Isl2-DTA retinas compared to control littermates. Bar graphs show the average number of ON (A) and OFF (B) RGCs found from white noise analysis (control, n=2; Isl2-DTA, n =4). Error bars = S.E.M.

It remains a possibility that the more common large, brisk transient type of RGCs, which were efficiently detected in Chapter 1, may drown out the signals produced by the rare RGC types. To determine if any rare RGC types can be detected in the absence of the Isl2 expressing RGCs, the ON type RGCs were classified using the RF diameter, STA time course and ACF as criteria to see what types of ON RGCs are detected in Is2-DTA retinas (see Chapter 1). Isl2-DTA ON classes fall into 2 broad categories: brisk, transient types and sluggish sustained types. This is similar to both Isl2 littermate control and C57BL/6 wild-type retinas. The RGCs that were part of a classified together do display mosaics (Figure 22). The OFF types were classified, but each class contained very few RGCs (Figure 23). Small types of ON RGCs were found, indicating that these types should also found in the wild-type retina. This shows that by eliminating the more dominant types of RGCs, detection of these small types by the MEA may be more efficient.

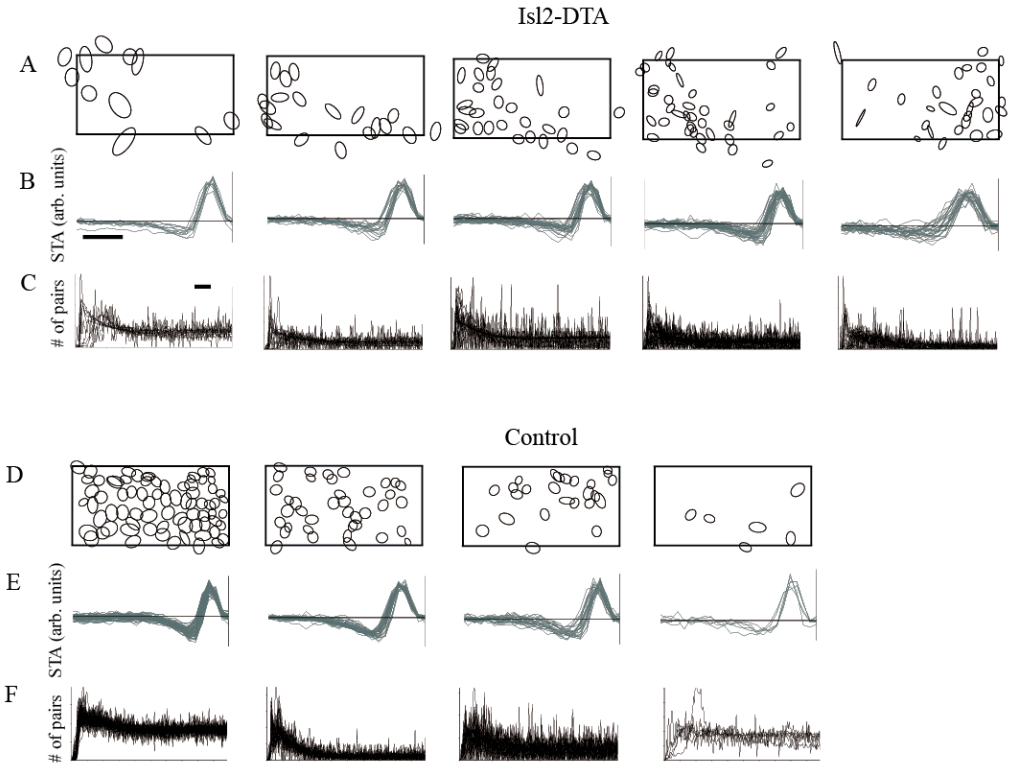

Figure 22. Small, sluggish, sustained ON classes are present in the retina. All ON classes identified in a single Isl2-DTA retina (A-C) or a single littermate control retina (D-F). Brisk/sluggish and transient/sustained types were found. (A) The RF overlay is shown for each Isl2-DTA ON RGC class (columns). (B) STA time courses are shown for each Isl2-DTA ON class. (C) Temporal ACF is shown for each Isl2-DTA ON class. Scale bar = 10ms. (D) The RF overlay is shown for each control ON RGC class (columns). Box represents the recording area of the MEA and is 1.7mm^2. (E) STA time courses are shown for each control ON class. Scale bar = 100ms. (F) Temporal ACF is shown for each control ON class. Box represents the recording area of the MEA and is 1.7mm^2. Scale bar for time course = 100ms. Scale bar for ACF = 10ms.

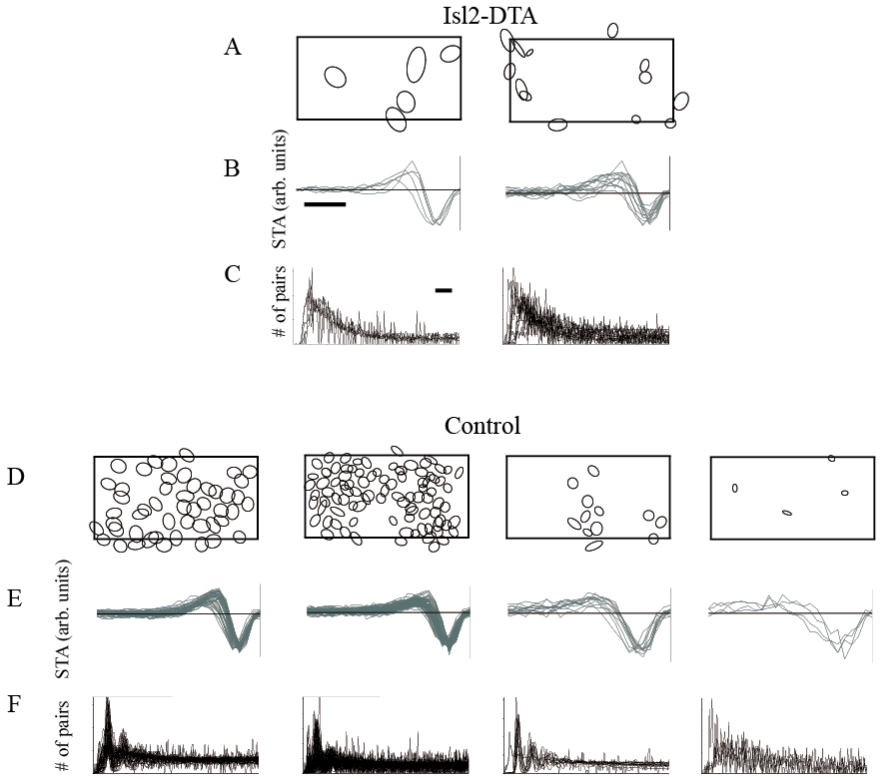

Figure 23. All OFF classes identified in a single Isl2-DTA retina (A-C) or a single littermate control retina (D-F). Brisk/sluggish and transient/sustained types were still found. (A) The RF overlay is shown for each Isl2-DTA OFF RGC class (columns). (B) STA time courses are shown for each Isl2-DTA OFF class. (C) Temporal ACF is shown for each Isl2-DTA OFF class. Scale bar = 10ms. (D) The RF overlay is shown for each control OFF RGC class (columns).. (E) STA time courses are shown for each control OFF class. Scale bar = 100ms. (F) Temporal ACF is shown for each control OFF class. Box represents the recording area of the MEA and is 1.7mm^2. Scale bar for time course = 100ms. Scale bar for ACF = 10ms.

Isl2-DTA mice have reduced projections to dLGN but not SCN

Different brain targets are responsible for processing different aspects of vision and behavior, which can indicate functional properties of the RGCs that project

to those brain regions. The Isl2-GFP labeled RGCs have been shown to project to the dLGN and the SC, but not to the SCN or other non-image forming visual centers in the adult mouse (Triplett et al., 2014). To determine where the remaining RGCs project in the brains of Isl2-DTA mice, I performed whole eye fills on 2 Isl2-DTA and 2 littermate control mice with the cholera toxin beta subunit conjugated to a fluorescent molecule to trace axonal projections in the brain. The left eye was filled with CTB-555 (red) and the right eye was filled with CTB-488 (green). In mice, 97-98% of RGCs project contralaterally (Drager and Olsen, 1980). Coronal brain sections were taken going anterior to posterior. Projections to the SCN and dLGN were examined and compared between Isl2-DTA and littermate controls.

The SCN was located in the hypothalamus, and can be seen in the medial-ventral area of the section. The observed fluorescence in the two nuclei in the Isl2-DTA brain sections was similar, which is also observed in the littermate control sections (Figure 24A). RGC project equal amounts of contralateral and ipsilateral projections to the SCN. Because there was no difference between the fluorescence observed between the two nuclei within a section, contralateral RGC that project to the SCN were preserved in the Isl2-DTA animals and were no specifically eliminated.

The dLGN was located in the thalamus and was present in sections slightly more posterior and dorsal than the SCN and laterally under the cortex. The observed fluorescence in the contralateral dLGN, shown by the green patch, was reduced in Isl2-DTA sections compared to littermate controls (Figure 22B). There was still

fluorescence in the contralateral dLGN suggesting that not all contralaterally projecting RGCs were eliminated. More sections must be analyzed in order to determine if all the Isl2-DTA contralateral projections terminate in a stereotypical region in the dLGN. Because 2-3% of RGCs project ipsilaterally, the ipsilateral dLGN was compared between control and Isl2-DTA mice (Drager and Olsen, 1980). Ipsilateral RGCs, as seen by the red patch, were observed in both Isl2-DTA and littermate control brain sections (Figure 24B). Ipsilateral patches seemed similar in both Isl2-DTA and controls. It was surprising to see that the ipsilateral patch was not expanded in the absence of the contralateral projections. These results suggest that Isl2 is expressed in contralaterally projecting RGCs that are involved in image forming pathways. Although some of the contralateral, image forming RGCs are missing in the Isl2-DTA mice, they might still be able to form images due to the preservation of the ipsilateral dLGN type of RGC.

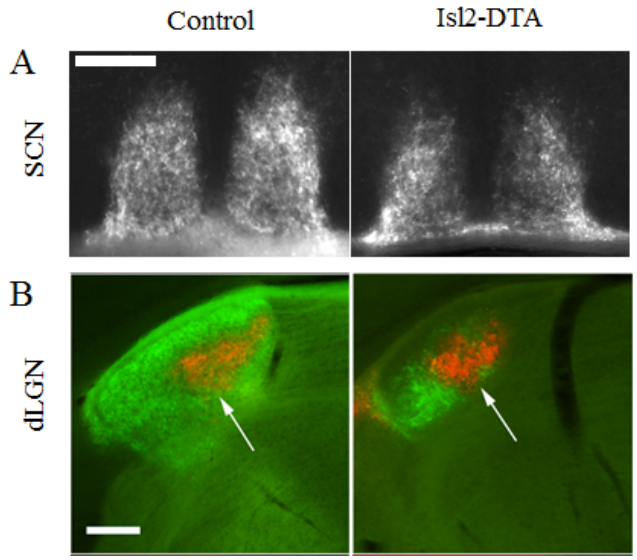

Figure 24. Whole eye fills in Isl2-DTA mice showed fewer contralateral projections to the dLGN, but not the SCN. The left eye was injected with CTB-555 (red) and the right eye was injected with CTB-488 (green) and coronal sections cut at 100µm slices are shown. (A) Littermate control and Isl2-DTA sections showing projections from one eye to the SCN, a non-image forming brain target. Only the red channel is shown. (B) Littermate control and Isl2-DTA sections showing projections to the dLGN, an image-forming brain target. Arrows point at the ipsilateral patch shown in red. Scale bar = 200µm.

Discussion

RGC development and fate determination are dependent on transcriptional regulation. The transcription factor, Isl2, is expressed in approximately 40% of all RGCs and has been found to be expressed specifically in contralateral RGC (Pak et al., 2004; Triplett et al., 2014). Here, Isl2 RGCs were eliminated around birth. Both electrophysiological and anatomical approaches were used to characterize RGC types that were spared when Isl2-DTA RGCs were ablated.

The Isl2-DTA mice were generated in which DTA was expressed under the genetic control of *CB2-Cre* and results in the ablation of cells that express DTA. CB2 is the *Calbindin-2* promoter, but the amount of overlap between Isl2 and CB2 in RGCs is not known. Here, I showed that cell death does occur suggesting that there is overlap between Isl2 and CB2. Future experiments using reporter mice or immunohistochemistry will have to be performed in order to determine what proportion of Isl2 RGCs also express CB2. Different Cre lines will also have to be utilized in order to induce DTA expression in Isl2 RGCs that do not express CB2.

Isl2-DTA mice exhibited a significant loss of RGC. The optic nerve diameter was nearly half as large in the Isl2-DTA mice as in controls. Additionally, the MEA data shows an overall reduction in the number of RGCs identified. Surprisingly, the amount of Brn3a labeled RGCs in whole mount retinas was highly reduced in the Isl2-DTA retina. Brn3a labels approximately 80% of all RGCs (Quina et al., 2005; Badea et al., 2009; Badea and Nathans, 2011; Nadal-Nicolas et al., 2012). Approximately 95% of all Isl2-GFP RGCs also express Brn3a (Triplett et al., 2014). If all Isl2 RGCs express Brn3a, then it is expected that about half of the Brn3a RGCs should still remain. However, more than half of the Brn3a label was reduced in the Isl2-DTA retinas. Isl2 has been shown to be expressed more widespread in the inner retinal layers early in embryonic development, but becomes restricted to the GCL (Pak et al., 2004). Because Cre is expressed during this refinement of Isl2, it is possible that *CB2-Cre* may be expressed in RGCs that initially express Isl2, but do not later in development. This would result in more RGC cell death that predicted by

the expression in the Isl2-GFP line. Different, retinal specific Cre mouse lines will need to be utilized in order to determine the extent and details of unspecific cell death in the Isl2-DTA retinas. Also, the RGCs that project ipsilaterally are located in the ventro-temporal crescent (VTC) in the retina (Pak et al., 2004). Whole-mount IHC will have to be performed on retinas, in which orientation is maintained, in order to see if Brn3a labeling is denser in the VTC.

Despite the possibility of excess cell death, Isl2-DTA retinas had specific RGC types spared. The Isl2-GFP data suggests that the over 80% of SMI-32 RGCs also express Isl2 (Triplett et al., 2014). The SMI-32 immunohistochemistry showed a reduction in labeled RGCs. Based on these results, the alpha RGCs may be one RGC type that was eliminated. Additionally, Isl2-GFP RGCs project to the image forming brain targets such as the dLGN. Here, the amount of fluorescence from whole eye fills indicated reduced projections to both the dLGN. The non-image forming RGC types do not overlap with Isl2, and were expected to be unaffected in the Isl2-DTA retinas. To support that hypothesis, the eye fill experiments show similar fluorescence in the SCN in controls and Isl2-DTA brains. One type of RGC that is known to project to the SCN is the melanopsin expressing ipRGC, which do not overlap with Isl2.

The most striking data was the electrophysiological results that showed a huge reduction in the OFF type RGCs, while the ON types remained. Typically, OFF type RGCs account for half or more than half of the classifiable RGCs (see Chapter 1).

This suggests that specific cell death occurred as ON and OFF types would be expected to be equally affected. The major cell types that are usually detected in MEA recordings of wild-type retinas are the OFF brisk, transient types. However, no OFF type RGCs could be classified due to such few OFF types being detected. Isl2-DTA did not disrupt the ON type RGCs in the same way as the OFF types. The non-image forming RGCs typically detect light onset, which could explain why the ON types were not affected as much by the loss of Isl2 RGCs (Provencio et al., 2000; Berson et al., 2002; Hattar et al., 2002). This would indicate that Isl2 may be involved establishing OFF type synapses or anatomy. The MEA approach offered a quick means of screening the functional properties of Isl2-DTA retinas in order to determine what channels are left. Because numerous RGC could be detected in a single preparation, the cell death in Isl2-DTA retinas could be observed physiologically. Also, specific cell types such as OFF types were shown to be specifically eliminated, while the ON types remained. Due to the reduction in some of the dominant types of RGCs, such as the OFF LBT and OFF MBT, it is possible that more rare RGC types may be detected with higher efficiency. Slower, sustained type RGCs seemed to be better detected in the Isl2-DTA retinas than controls. This will assist in generating a functional classification of RGCs.

Overall, my data suggests that Isl2 specifies a subset of RGCs that include the OFF type RGCs that project contralaterally to image forming brain targets. This study lends support to the role of Isl2 in generating image forming, but not non-image forming RGCs, involved in contrast detection. Isl2 may act upstream of other

transcription factors as 40% of all RGCs may express it in the adult mouse, which suggests that this subset includes multiple cell types. Like Isl2, other transcription factors such as Tbr2, have also been shown to specify specific subsets of RGCs (Sweeney et al., 2014). The roles of transcription factors like Isl2 will be important in understanding RGC development and fate determination. With knowledge of the transcription code, better and more specific diagnoses and treatments for retinal diseases can be developed, as affected cell types and circuits can be identified and analyzed.

Conclusions

To understand what information the retina extracts and sends to the brain, I show how anatomy, physiology and genetics can be combined to describe the different pathways involved in feature detection. Using the 512 MEA and the mouse as a model system, I first characterized and classified RGCs in the wild-type retina, and then compared genetically manipulated mice to wild-types to determine how certain genes affect the morphology and response properties of those RGC classes. In order to develop a powerful classification, each RGC will have to be described as having a defined morphology, preferred stimuli and set of genes that when expressed results in the morphological and functional features of a particular class. My work will lead to such a classification by pioneering the effort to relate morphological and anatomical changes, due to genetic manipulation, to functional changes.

Functional classifications in the adult wild-type mouse

Before the functional changes in mutant or transgenic mouse RGCs can be compared to wild-type, a reliable functional classification of wild-type RGCs needed to be developed. In addition to detecting multiple cell types in the same preparation, recording from large numbers of RGCs allows for observations of RF mosaics. Mosaics have been used to determine if a population of RGCs is indeed a unique class of RGCs (Wassle et al., 1981; Rodieck, 1991; Rodieck and Marshak, 1992; Dacey, 1993b; Devries and Baylor, 1997; Field et al., 2007; Petrusca et al., 2007;

Gauthier et al., 2009; Anishchenko et al., 2010; Sher and DeVries, 2012). I used these mosaics as a verification of my classifications, as well as an expected feature of wild-type RGCs.

From the wild-type recordings, I was able to classify up to 8 different cell types. I was able to reliably identify 2 OFF and 2 ON RGC types using white noise stimulus. At least 4 types of DSRGCs could be detected. These classes of RGCs can be used to answer simple questions, such as if mosaics are disrupted or if DSRGCs were present in a mutant retina. These classes were the best ones that I could detect in the wild-type mouse using the 512 MEA. Other white noise classes exist, but mosaics were too incomplete to be absolutely sure they represent different classes. It remains to be seen how many more white noise classes exist.

Based on my classification nomenclature, 12 ON and 12 OFF types are possible given the different permutations. This would be over the predicted number of RGCs, though. There are about 8 types of DSRGCs that have been previously described and 5 types of ipRGCs (Barlow and Hill, 1963; Barlow and Levick, 1965; Oyster and Barlow, 1967; Provencio et al., 2000; Hattar et al., 2002; Chen et al., 2011). However, not all of the possible white noise classes may be true classes. Recently, alpha or alpha-like RGCs have been shown to vary in dendritic and receptive field size in a nasal to temporal gradient in the mouse retina (Bleckert et al., 2014). This suggests that RGCs with similar properties other than RF size may represent the same class. Due to recording inefficiencies that result in gaps in

coverage of RFs, it is hard to determine if these classes with different RF sizes represents one class or multiple classes. Indeed in at least a few recordings, the two classes can be put together and the RFs form a complete mosaic across the array's recording area.

The current classification does allow for comparisons of genetically manipulated retinas as well as describing basic feature detectors. This wild-type classification was generated using simple stimuli that produced a wealth of data about some of the major types of RGCs, contrast detectors and direction selective detectors. Mutant analysis will show how the removal or alteration of the feature detectors affects behavior. Eventually, my work will lead an understanding of how each feature detector in the retina contributes to visual perception and behavior.

DSCAM is required for RF arrangement and direction selective responses of RGCs

The *DSCAM*$^{-/-}$ mouse presented the opportunity to directly test how the anatomical features of an RGC type relates to its functional properties. The absence of DSCAM in the mouse retina leads to the anatomical clumping of dendrites and cell bodies of RGCs that are part of a unique class. Additionally, subsets of amacrine cells also display the clumping phenotype (Fuerst et al., 2008; Fuerst et al., 2009; Fuerst et al., 2010; Keeley et al., 2012; de Andrade et al., 2014). The anatomical defects in the *DSCAM*$^{-/-}$ retina allowed me to directly compare the functional properties that were derived from the classification from wild-type retinas.

Despite, the severe clumping phenotype, RGC response properties were largely normal in the brisk, transient cell types. ON and OFF RGC types were found and the RF diameter was not different compared to controls (Figure 25). This confirmed that the RGC clumps did not result in non-functional RGCs and the mice were not completely blind. The only difference that could be identified was in the time to zero, which was slower in *DSCAM*$^{-/-}$ RGC classes. This suggests that the number or density of synapses was most likely altered, which could affect the response kinetics. It does remain a possibility that more subtle properties may be affected, and more detailed analysis will have to be performed.

RF mosaics were disrupted in all RGC classes that I detected in the *DSCAM*$^{-/-}$ retinas. This confirmed that the spatial position of an RGC's RF depends upon the anatomical positioning of the RGC within the 2D layer of the GCL. This supports the hypothesis that the position of the RGC dictates the synaptic connections that the RGC makes with the upstream retinal neurons. In early development, RGCs are part of the early born neurons in the retina (Reese, 2011). Initially, the RGCs in the DSCAM retina do not show any differences with wild-type retinas until P4 (Fuerst et al., 2008). It is a possibility that when same type RGCs clump, their dendrites form connections within their new vicinity. This would determine where the spatial RF will be positioned.

The clumped dendritic phenotype disrupted DSRGC function in the DSCAM$^{-/-}$ retinas. ON-OFF direction selective responses depend on complex circuitry that

depends on dendritic connections between the DSRGCs with four starburst amacrine and bipolar cells (Demb, 2007; Wei and Feller, 2011; Wei et al., 2011). This indicates the importance of the dendritic structure in making the proper connections that generate direction selective responses. The absence of DSCAM may reduce the chances of an ON-OFF DSRGC from making all the necessary synapses (Figure 24). It will be important to test behavioral aspects of the *DSCAM*$^{-/-}$ mice to confirm the lack of direction selective behaviors. The results from the DS analysis suggest that more complex circuits such as the DS circuits are more affected by dendritic abnormalities than simple ON and OFF circuits.

The work I performed in the *DSCAM*$^{-/-}$ retina supports how anatomy dictates the functional properties of the RGC and how the MEA can be used to correlate function to anatomy. This was the first time that a mutant phenotype was identified on the MEA. Differences between wild-type and *DSCAM*$^{-/-}$ retinas can be detected using just two stimuli, the white noise and moving bars movies.

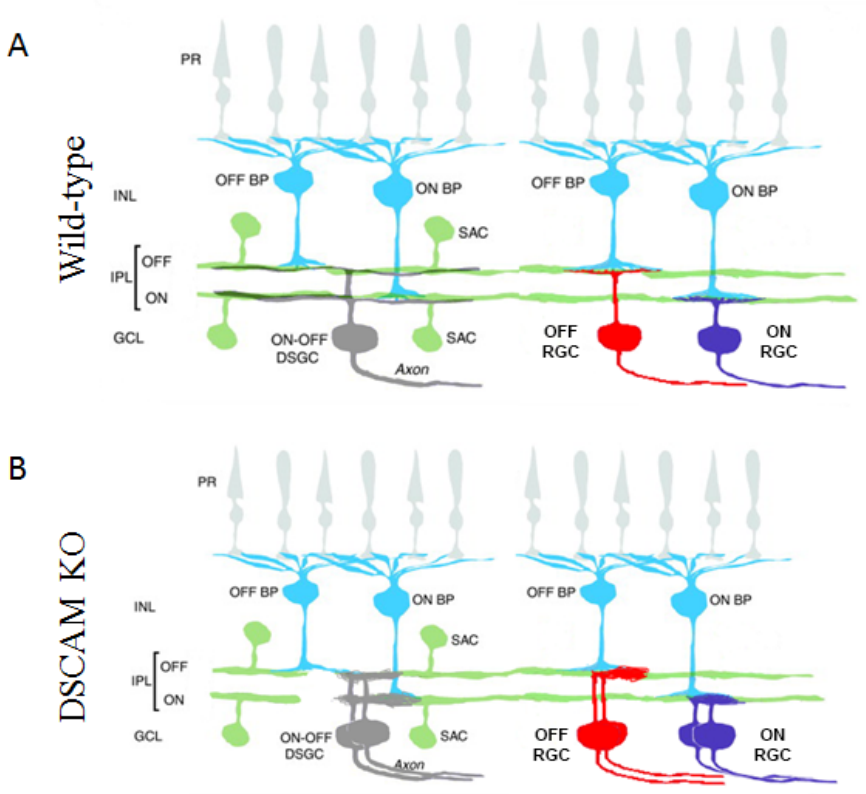

Figure 25. DSRGC have more complex circuitry than ON or OFF type RGCs (adapted from Wei and Feller, 2011). (A) Wild-type circuitry is shown for an ON-OFF DSRGC (gray cell in GCL), an OFF RGC (red cell in GCL) and an ON RGC (dark blue). The ON-OFF DSRGC must make 6 synapses: ON bipolar, OFF bipolar and 4 SACs. (B) Potential clumping effects in *DSCAM*$^{-/-}$ mice. ON-OFF DSRGC (gray cell in GCL) has less of a chance to reliably make all 6 synapses, while ON or OFF RGCs can still contact the respective bipolar cell. ON or OFF RGCs may share the same upstream circuitry that can result in clumped RFs.

Characterization of remaining RGCs in the Isl2-DTA retina

The Isl2-DTA mouse enabled me to examine the RGC types that remain after the ablation of a subset of RGCs. Previously, the genetic activation of DTA was used to specifically ablate the melanopsin expressing ipRGCs (Chen et al., 2011; Zhang et

al., 2012). These previous studies identified behavioral defects directly showing the role of the ipRGCs in visual perception and behavior. Using a similar approach, Isl2 RGCs were ablated with the DTA and the remaining RGC were analyzed both anatomically and physiologically.

Using the Isl2-DTA mouse, I was able to ablate specific visual channels in order to understand how genetics is related to morphology and physiology. I found that the RGCs that were eliminated were specifically OFF type RGCs. In normal retinas, such as littermate controls or wild-type mice, there are similar numbers of ON and OFF type RGCs. The lack of OFF type RGCs in the Isl2-DTA retinas indicates that Isl2 may be involved in the development or generation of contralateral OFF type RGCs, as Isl2 is only expressed in contralateral RGCs (Pak et al., 2004).

In order to get an idea of what behaviors the Isl2 expressing RGCs mediate, I traced the projections of the remaining RGCs in Isl2-DTA animals to image forming and non-image forming brain targets. The contralateral projections to the SCN were preserved, but not those to the dLGN. This suggests that Isl2 can be used to distinguish between these two sets of RGCs. These results are preliminary, and different brain regions such as the superior colliculus must be analyzed in more detail. So far, I only described two brain targets for RGCs, the dLGN and the SCN. The Isl2-GFP line can give clues for other brain targets as GFP labeled axons project to image forming brain targets, but not non-image forming targets in the adult mouse (Triplett et al., 2014). It remains to be seen if the Isl2-DTA recapitulates what is predicted

about the projections in the Isl2-GFP. These observations suggest that the Isl2 expressing RGCs are involved in image forming visual processes and behaviors. Together with the physiology data, I show how gene expression can be used to define specific subsets of RGCs, thus contributing to the overall goal of understanding the development and function of the different channels in the retina.

Final remarks

The 512 MEA electrophysiological approach is a simple way to analyze large populations of neurons in a single preparation. Here, I show the utility of this approach in classifying RGCs and screening genetically manipulated retinas. The MEA allowed me to test how morphology and function are linked. Identification of genes involved in the generation of RGCs will be important in understanding how the retina functions as a whole and how to develop better treatments for retinal disease or visual defects.

The mechanisms of RGC development and function are important to how visual processes enable the vivid imagery that we perceive, as well as how light affects our behaviors. The activity of the RGCs is all the information that is sent to the brain. By analyzing the signals sent to the brain from the retina, the neural code can be deciphered as the input stimulus and output response are well defined and easily measured. This will not only be helpful in understanding how the retina

encodes information, but how the entire nervous system represents and perceives the information.

Bibliography

Anishchenko A, Greschner M, Elstrott J, Sher A, Litke AM, Feller MB, Chichilnisky EJ (2010) Receptive field mosaics of retinal ganglion cells are established without visual experience. J Neurophysiol 103:1856-1864.

Badea TC, Nathans J (2011) Morphologies of mouse retinal ganglion cells expressing transcription factors Brn3a, Brn3b, and Brn3c: analysis of wild type and mutant cells using genetically-directed sparse labeling. Vision Res 51:269-279.

Badea TC, Cahill H, Ecker J, Hattar S, Nathans J (2009) Distinct roles of transcription factors brn3a and brn3b in controlling the development, morphology, and function of retinal ganglion cells. Neuron 61:852-864.

Barlow HB, Hill RM (1963) Selective sensitivity to direction of movement in ganglion cells of the rabbit retina. Science 139:412-414.

Barlow HB, Levick WR (1965) The mechanism of directionally selective units in rabbit's retina. J Physiol 178:477-504.

Berson DM (2003) Strange vision: ganglion cells as circadian photoreceptors. Trends Neurosci 26:314-320.

Berson DM (2008) Retinal Ganglion Cell Types and Their Central Projections. In: The Senses: A Comprehensive Reference (Basbaum A, Shepherd G, Westheimer G, eds), pp 491-520. San Diego: Academic Press.

Berson DM, Dunn FA, Takao M (2002) Phototransduction by retinal ganglion cells that set the circadian clock. Science 295:1070-1073.

Blank M, Fuerst PG, Stevens B, Nouri N, Kirkby L, Warrier D, Barres BA, Feller MB, Huberman AD, Burgess RW, Garner CC (2011) The Down syndrome critical region regulates retinogeniculate refinement. J Neurosci 31:5764-5776.

Bleckert A, Schwartz GW, Turner MH, Rieke F, Wong RO (2014) Visual space is represented by nonmatching topographies of distinct mouse retinal ganglion cell types. Curr Biol 24:310-315.

Boycott BB, Wassle H (1974) The morphological types of ganglion cells of the domestic cat's retina. J Physiol 240:397-419.

Brown NL, Patel S, Brzezinski J, Glaser T (2001) Math5 is required for retinal ganglion cell and optic nerve formation. Development 128:2497-2508.

Carroll K, Gomez C, Shapiro L (2004) Tubby proteins: the plot thickens. Nat Rev Mol Cell Biol 5:55-63.

Chen SK, Badea TC, Hattar S (2011) Photoentrainment and pupillary light reflex are mediated by distinct populations of ipRGCs. Nature 476:92-95.

Chichilnisky EJ (2001) A simple white noise analysis of neuronal light responses. Network 12:199-213.

Chichilnisky EJ, Kalmar RS (2002) Functional asymmetries in ON and OFF ganglion cells of primate retina. J Neurosci 22:2737-2747.

Clandinin TR, Feldheim DA (2009) Making a visual map: mechanisms and molecules. Curr Opin Neurobiol 19:174-180.

Coombs J, van der List D, Wang GY, Chalupa LM (2006) Morphological properties of mouse retinal ganglion cells. Neuroscience 140:123-136.

Dacey DM (1993a) Morphology of a small-field bistratified ganglion cell type in the macaque and human retina. Vis Neurosci 10:1081-1098.

Dacey DM (1993b) The mosaic of midget ganglion cells in the human retina. J Neurosci 13:5334-5355.

Dacey DM (1999) Primate retina: cell types, circuits and color opponency. Prog Retin Eye Res 18:737-763.

Dacey DM (2004) Origins of Perception: Retinal Ganglion Cell Diversity and the Creation of Parallel Visual Pathways. In: The cognitive neurosciences III (MS G, ed), pp 281-301. Cambridge, MA: MIT press.

de Andrade GB, Long SS, Fleming H, Li W, Fuerst PG (2014) DSCAM localization and function at the mouse cone synapse. J Comp Neurol.

Demb JB (2007) Cellular mechanisms for direction selectivity in the retina. Neuron 55:179-186.

Devries SH, Baylor DA (1997) Mosaic arrangement of ganglion cell receptive fields in rabbit retina. J Neurophysiol 78:2048-2060.

Drager UC, Olsen JF (1980) Origins of crossed and uncrossed retinal projections in pigmented and albino mice. J Comp Neurol 191:383-412.

Elstrott J, Anishchenko A, Greschner M, Sher A, Litke AM, Chichilnisky EJ, Feller MB (2008) Direction selectivity in the retina is established independent of visual experience and cholinergic retinal waves. Neuron 58:499-506.

Erkman L, McEvilly RJ, Luo L, Ryan AK, Hooshmand F, O'Connell SM, Keithley EM, Rapaport DH, Ryan AF, Rosenfeld MG (1996) Role of transcription factors Brn-3.1 and Brn-3.2 in auditory and visual system development. Nature 381:603-606.

Farrow K, Masland RH (2011) Physiological clustering of visual channels in the mouse retina. J Neurophysiol 105:1516-1530.

Field GD, Sher A, Gauthier JL, Greschner M, Shlens J, Litke AM, Chichilnisky EJ (2007) Spatial properties and functional organization of small bistratified ganglion cells in primate retina. J Neurosci 27:13261-13272.

Fuerst PG, Koizumi A, Masland RH, Burgess RW (2008) Neurite arborization and mosaic spacing in the mouse retina require DSCAM. Nature 451:470-474.

Fuerst PG, Harris BS, Johnson KR, Burgess RW (2010) A novel null allele of mouse DSCAM survives to adulthood on an inbred C3H background with reduced phenotypic variability. Genesis 48:578-584.

Fuerst PG, Bruce F, Tian M, Wei W, Elstrott J, Feller MB, Erskine L, Singer JH, Burgess RW (2009) DSCAM and DSCAML1 function in self-avoidance in multiple cell types in the developing mouse retina. Neuron 64:484-497.

Fukuda Y, Hsiao CF, Watanabe M, Ito H (1984) Morphological correlates of physiologically identified Y-, X-, and W-cells in cat retina. J Neurophysiol 52:999-1013.

Gauthier JL, Field GD, Sher A, Greschner M, Shlens J, Litke AM, Chichilnisky EJ (2009) Receptive fields in primate retina are coordinated to sample visual space more uniformly. PLoS Biol 7:e1000063.

Guler AD, Altimus CM, Ecker JL, Hattar S (2007) Multiple photoreceptors contribute to nonimage-forming visual functions predominantly through melanopsin-containing retinal ganglion cells. Cold Spring Harb Symp Quant Biol 72:509-515.

Hattar S, Liao HW, Takao M, Berson DM, Yau KW (2002) Melanopsin-containing retinal ganglion cells: architecture, projections, and intrinsic photosensitivity. Science 295:1065-1070.

Herrera E, Brown L, Aruga J, Rachel RA, Dolen G, Mikoshiba K, Brown S, Mason CA (2003) Zic2 patterns binocular vision by specifying the uncrossed retinal projection. Cell 114:545-557.

Huberman AD, Feller MB, Chapman B (2008a) Mechanisms underlying development of visual maps and receptive fields. Annu Rev Neurosci 31:479-509.

Huberman AD, Wei W, Elstrott J, Stafford BK, Feller MB, Barres BA (2009) Genetic identification of an On-Off direction-selective retinal ganglion cell subtype reveals a layer-specific subcortical map of posterior motion. Neuron 62:327-334.

Huberman AD, Manu M, Koch SM, Susman MW, Lutz AB, Ullian EM, Baccus SA, Barres BA (2008b) Architecture and activity-mediated refinement of axonal

projections from a mosaic of genetically identified retinal ganglion cells. Neuron 59:425-438.

Kay JN, De la Huerta I, Kim IJ, Zhang Y, Yamagata M, Chu MW, Meister M, Sanes JR (2011) Retinal ganglion cells with distinct directional preferences differ in molecular identity, structure, and central projections. J Neurosci 31:7753-7762.

Keeley PW, Sliff BJ, Lee SC, Fuerst PG, Burgess RW, Eglen SJ, Reese BE (2012) Neuronal clustering and fasciculation phenotype in Dscam- and Bax-deficient mouse retinas. J Comp Neurol 520:1349-1364.

Kim IJ, Zhang Y, Yamagata M, Meister M, Sanes JR (2008) Molecular identification of a retinal cell type that responds to upward motion. Nature 452:478-482.

Kong JH, Fish DR, Rockhill RL, Masland RH (2005) Diversity of ganglion cells in the mouse retina: unsupervised morphological classification and its limits. J Comp Neurol 489:293-310.

Kuffler SW (1953) Discharge patterns and functional organization of mammalian retina. J Neurophysiol 16:37-68.

Litke AM, Bezayiff N, Chichilnisky EJ, Cunningham W, Dabrowski W, Grillo AA, Grivich MI, Grybos P, Hottowy P, Kachiguine S, Kalmar RS, Mathieson K, Petrusca D, Rahman SM, Sher A (2004) What does the eye tell the brain?: Development of a system for the large-scale recording of retinal output activity. IEEE Transactions on Nuclear Science 51:1434-1440.

Masland RH (2012) The neuronal organization of the retina. Neuron 76:266-280.

Matsuoka RL, Nguyen-Ba-Charvet KT, Parray A, Badea TC, Chedotal A, Kolodkin AL (2011) Transmembrane semaphorin signalling controls laminar stratification in the mammalian retina. Nature 470:259-263.

Maxwell F, Maxwell IH, Glode LM (1987) Cloning, sequence determination, and expression in transfected cells of the coding sequence for the tox 176 attenuated diphtheria toxin A chain. Mol Cell Biol 7:1576-1579.

Meister M, Pine J, Baylor DA (1994) Multi-neuronal signals from the retina: acquisition and analysis. J Neurosci Methods 51:95-106.

Millard SS, Flanagan JJ, Pappu KS, Wu W, Zipursky SL (2007) Dscam2 mediates axonal tiling in the Drosophila visual system. Nature 447:720-724.

Nadal-Nicolas FM, Jimenez-Lopez M, Salinas-Navarro M, Sobrado-Calvo P, Alburquerque-Bejar JJ, Vidal-Sanz M, Agudo-Barriuso M (2012) Whole number, distribution and co-expression of brn3 transcription factors in retinal ganglion cells of adult albino and pigmented rats. PLoS One 7:e49830.

Nassi JJ, Callaway EM (2009) Parallel processing strategies of the primate visual system. Nat Rev Neurosci 10:360-372.

Oesch N, Euler T, Taylor WR (2005) Direction-selective dendritic action potentials in rabbit retina. Neuron 47:739-750.

Osterhout JA, Josten N, Yamada J, Pan F, Wu SW, Nguyen PL, Panagiotakos G, Inoue YU, Egusa SF, Volgyi B, Inoue T, Bloomfield SA, Barres BA, Berson DM, Feldheim DA, Huberman AD (2011) Cadherin-6 mediates axon-target matching in a non-image-forming visual circuit. Neuron 71:632-639.

Oyster CW, Barlow HB (1967) Direction-selective units in rabbit retina: distribution of preferred directions. Science 155:841-842.

Pak W, Hindges R, Lim YS, Pfaff SL, O'Leary DD (2004) Magnitude of binocular vision controlled by islet-2 repression of a genetic program that specifies laterality of retinal axon pathfinding. Cell 119:567-578.

Pang JJ, Gao F, Wu SM (2003) Light-evoked excitatory and inhibitory synaptic inputs to ON and OFF alpha ganglion cells in the mouse retina. J Neurosci 23:6063-6073.

Peichl L (1991) Alpha ganglion cells in mammalian retinae: common properties, species differences, and some comments on other ganglion cells. Vis Neurosci 7:155-169.

Peichl L, Ott H, Boycott BB (1987) Alpha ganglion cells in mammalian retinae. Proc R Soc Lond B Biol Sci 231:169-197.

Petrusca D, Grivich MI, Sher A, Field GD, Gauthier JL, Greschner M, Shlens J, Chichilnisky EJ, Litke AM (2007) Identification and characterization of a Y-like primate retinal ganglion cell type. J Neurosci 27:11019-11027.

Provencio I, Rodriguez IR, Jiang G, Hayes WP, Moreira EF, Rollag MD (2000) A novel human opsin in the inner retina. J Neurosci 20:600-605.

Purves D (2008) Neuroscience, 4th Edition. Sunderland, Mass.: Sinauer.

Quina LA, Pak W, Lanier J, Banwait P, Gratwick K, Liu Y, Velasquez T, O'Leary DD, Goulding M, Turner EE (2005) Brn3a-expressing retinal ganglion cells project specifically to thalamocortical and collicular visual pathways. J Neurosci 25:11595-11604.

Reese BE (2011) Development of the retina and optic pathway. Vision Res 51:613-632.

Remtulla S, Hallett PE (1985) A schematic eye for the mouse, and comparisons with the rat. Vision Res 25:21-31.

Rodieck RW (1991) The density recovery profile: a method for the analysis of points in the plane applicable to retinal studies. Vis Neurosci 6:95-111.

Rodieck RW, Marshak DW (1992) Spatial density and distribution of choline acetyltransferase immunoreactive cells in human, macaque, and baboon retinas. J Comp Neurol 321:46-64.

Schramm RD, Li S, Harris BS, Rounds RP, Burgess RW, Ytreberg FM, Fuerst PG (2012) A Novel Mouse Dscam Mutation Inhibits Localization and Shedding of DSCAM. PLoS One 7:e52652.

Sher A, DeVries SH (2012) A non-canonical pathway for mammalian blue-green color vision. Nat Neurosci 15:952-953.

Sher A, Jones BW, Huie P, Paulus YM, Lavinsky D, Leung LS, Nomoto H, Beier C, Marc RE, Palanker D (2013) Restoration of retinal structure and function after selective photocoagulation. J Neurosci 33:6800-6808.

Shirasaki R, Pfaff SL (2002) Transcriptional codes and the control of neuronal identity. Annu Rev Neurosci 25:251-281.

Shlens J, Field GD, Gauthier JL, Grivich MI, Petrusca D, Sher A, Litke AM, Chichilnisky EJ (2006) The structure of multi-neuron firing patterns in primate retina. J Neurosci 26:8254-8266.

Stafford BK, Sher A, Litke AM, Feldheim DA (2009) Spatial-temporal patterns of retinal waves underlying activity-dependent refinement of retinofugal projections. Neuron 64:200-212.

Sun W, Li N, He S (2002) Large-scale morphological survey of mouse retinal ganglion cells. J Comp Neurol 451:115-126.

Sweeney NT, Tierney H, Feldheim DA (2014) Tbr2 is required to generate a neural circuit mediating the pupillary light reflex. J Neurosci 34:5447-5453.

Trenholm S, Johnson K, Li X, Smith RG, Awatramani GB (2011) Parallel mechanisms encode direction in the retina. Neuron 71:683-694.

Triplett JW, Wei W, Gonzalez C, Sweeney NT, Huberman AD, Feller MB, Feldheim DA (2014) Dendritic and axonal targeting patterns of a genetically-specified class of retinal ganglion cells that participate in image-forming circuits. Neural development 9:2.

Volgyi B, Chheda S, Bloomfield SA (2009) Tracer coupling patterns of the ganglion cell subtypes in the mouse retina. J Comp Neurol 512:664-687.

Wassle H (2004) Parallel processing in the mammalian retina. Nat Rev Neurosci 5:747-757.

Wassle H, Boycott BB (1991) Functional architecture of the mammalian retina. Physiol Rev 71:447-480.

Wassle H, Boycott BB, Illing RB (1981) Morphology and mosaic of on- and off-beta cells in the cat retina and some functional considerations. Proc R Soc Lond B Biol Sci 212:177-195.

Wassle H, Puller C, Muller F, Haverkamp S (2009) Cone contacts, mosaics, and territories of bipolar cells in the mouse retina. J Neurosci 29:106-117.

Wei W, Feller MB (2011) Organization and development of direction-selective circuits in the retina. Trends Neurosci 34:638-645.

Wei W, Hamby AM, Zhou K, Feller MB (2011) Development of asymmetric inhibition underlying direction selectivity in the retina. Nature 469:402-406.

Williams SE, Mann F, Erskine L, Sakurai T, Wei S, Rossi DJ, Gale NW, Holt CE, Mason CA, Henkemeyer M (2003) Ephrin-B2 and EphB1 mediate retinal axon divergence at the optic chiasm. Neuron 39:919-935.

Zhang J, Wei H, Guo X, Hu M, Gao F, Li L, Zhang S (2012) Functional verification of the diphtheria toxin A gene in a recombinant system. Journal of animal science and biotechnology 3:29.